Aus dem Institute of Regenerative Biology and Medicine, Helmholtz Center Munich und Ludwig-Maximilians-Universität München

Dissertation

zum Erwerb des Doctor of Philosophy

(Ph.D.) an der Medizinischen Fakultät der Ludwig-Maximilians-Universität zu München

# *AAV-mediated gene delivery in the cutaneous wound healing*

vorgelegt von:

.Shaohua Zhu.

aus:

Anhui, China

Jahr:

2023

Mit Genehmigung der Medizinischen Fakultät der
Ludwig-Maximilians-Universität zu München

| | |
|---|---|
| **First supervisor:** | Dr. Yuval Rinkevich |
| **Second supervisor:** | Prof. Dr. med. Jürgen Behr |
| **Third evaluator** | Prof. Dr. Stylianos Michalakis |
| **Forth evaluator** | apl. Prof. Dr. Daniela Hartmann |

**Dean:** **Prof. Dr. med. Thomas Gudermann**

date of the defense:

_____02.03.2023_____

# Table of content

Table of content ..... 4
Abstract ..... 9
List of figure ..... 10
List of Tables ..... 10
Abbreviations ..... 11
1 Introduction ..... 13
1.1 Adeno-associated viral vectors ..... 13
1.1.1 The genomic structure of AAV ..... 13
1.1.2 The diagram of the AAV transduction pathway ..... 15
1.1.3 The AAV serotype and the capsid engineering ..... 18
1.1.4 The main challenge of AAV in the application of gene therapy ..... 20
1.1.5 The application of AAV vector for in vitro gene transfer ..... 22
1.2 Wound healing ..... 23
1.2.1. The anatomy and functions of the skin ..... 23
1.2.3 Fibroblast Heterogeneity in Skin Wound Healing ..... 28
1.3 The role of Ak1c18 family members and progesterone in wound healing ..... 29
1.4 The aim of the thesis ..... 31
2 Experiment materials ..... 33
2.1 Cell lines used in this project ..... 33
2.2 laboratory equipment ..... 33
2.3 Culture media, buffers, solutions and reagents ..... 34
2.4 Kits and Enzyme ..... 34
2.5 Chemical and solution ..... 35
2.6 Laboratory animals ..... 35
2.7 Bacterial strains ..... 36
3. Methods ..... 36
3.1 The design of cloning primers. ..... 36
3.2 Restriction digestion reaction ..... 37

3.3 Ligation reaction ..... 37
3.4 Transformation ..... 38
3.5 Infusion cloning ..... 38
3.6 AAV production and purification ..... 39
3.7 Virus titration ..... 40
3.8 Realtime PCR ..... 41
3.8.1 Extraction of cellular RNA (6-well plate) ..... 41
3.8.2 Reverse transcription ..... 41
3.9 Full-thickness excisional wound model in mice ..... 42
3.10 Scar-in-a-dish (SCAD) assay ..... 42
3.11 Live imaging of cell migration ..... 43
3.12 Histology ..... 44
3.12.1 Cryosection ..... 44
3.12.2 Immunofluorescence ..... 44
3.12.3 Masson's Trichrome staining ..... 45
3.13 Statistical analysis ..... 46
3.14 Bioinformatic analysis ..... 46
3.14.1. Sample preparation ..... 46
3.14.2. Bioinformatic process of the single-cell RNA sequencing data ..... 47
4 Results ..... 47
4.1 Characterization of an ex vivo wound healing model termed SCAR in a dish (SCAD). ..... 48
4.2 AAV6-mediated transgene overexpression in SCADs ..... 50
4.3 Sodium butyrate is used to boost AAV transfection for in vitro ..... 52
4.4 Design optimization of the AAV transgene construct ..... 54
4.4.1 Linker is not suitable for the co-expression of GFP and target gene using the AAV system. ..... 54
4.4.2 2A self-cleavage peptide enables efficient co-expression of GFP and Akr1c18 ex vivo ..... 56
4.5 Investigate the role of Akr1c18 in wound healing in the SCAD model ..... 58
4.6 Investigate the role of Akr1c18 in wound healing in the excisional wound model ..... 60
4.7 Bioinformatic analysis Akr1c18 expression pattern during the wound healing 61

5. Discussions ..... 64
5.1 Transduction optimization of AAV vectors for in vitro application ..... 64
5. 2 The importance of the proper design of AAV transgenic plasmids, which is often overlooked. ..... 65
5.3 The role of Akr1c18 and progesterone in wound healing. ..... 67
Reference ..... 69
Acknowledgment ..... 74
Affidavit ..... 76
Confimation of congruency ..... 77
List of Publication ..... 78

# Zusammenfassung

Die Wundheilung der Haut ist ein komplexer physiologischer Prozess, an dem verschiedene Zellen wie Immunzellen, Fibroblasten und Keratinozyten beteiligt sind. Eine gestörte Heilung von Hautverletzungen, wie z. B. chronische Wunden durch Diabetes oder übermäßige Narbenbildung, stellt eine enorme Belastung für Patienten und Gesellschaft dar. AAV wird häufig in Tierversuchen in der biologischen Forschung eingesetzt und ist auch ein ideales Instrument für die Gentherapie beim Menschen. Im Bereich der Reparatur von Hautverletzungen wird AAV jedoch nur selten eingesetzt. Unser Ziel ist es, die Effizienz und Spezifität der Genübertragung auf die Haut durch AAV-Vektoren zu verbessern und Lösungen zu finden, um die Narbenbildung zu verringern und die Regeneration bei der Wundheilung der Haut zu fördern.

Zunächst haben wir die Transfektionseffizienz des In-vitro-Narbenmodells SCAD (Narbe in der Schale) verbessert. Es wird allgemein angenommen, dass die genetische Manipulation mit AAV-Vektoren hauptsächlich auf Tierversuche beschränkt ist und nur selten in In-vitro-Studien vorkommt. Obwohl die SCAD-Proben mit dem AAV6-Serotyp mit hoher Transfektionseffizienz transfizierbar zu sein schienen, wie 3D-Bilder von anderen Labormitgliedern zeigten, stellten wir fest, dass die tatsächliche Effizienz extrem niedrig war. Selbst mit einer Erhöhung der verwendeten Virusmenge oder der Verwendung von AAV-DJ (ein Serotyp, der in einer Vielzahl von Zelllinien gut funktioniert) bleibt dieses Problem ungelöst. Wir fanden heraus, dass Natriumbutyrat, ein Histon-Deacetylase-

Inhibitor, die Transfektionseffizienz von SCAD-Gewebe um mindestens das 20- bis 50-faltet verbessern. Wir haben auch einige Arbeiten zur Optimierung des Designs der transgenen Plasmide durchgeführt. Wir fanden heraus, dass bei Verwendung eines Fusionsproteins aus GFP und dem Zielgen die GFP-Expression zu gering war, um erkannt zu werden. Durch die Anwendung der 2A selbstreinigenden Peptid-vermittelten Koexpression von GFP und Zielgenen konnte das Problem der geringen Transfektion überwunden werden, was die Verfolgung der Zellmigration im SCAD-Modell erleichtert.

Akr1c18 ist eine Steroiddehydrogenase und fungiert als Progesteron-Inaktivator. Die Expression von Akr1c18 ging während der Wundheilung entlang einer pseudotemporalen Trajektorie stark zurück und könnte den Progesteronspiegel in der Haut regulieren. Die Einzelzelldaten zeigten außerdem, dass Akr1c18 in Pro-Myofibroblasten stark, in reifen Wundfibroblasten jedoch nur schwach exprimiert wird. Wir waren daran interessiert, herauszufinden, dass Akr1c18 eine gewisse Wirkung auf die geschwollene Faszie und die Fibroblastenmigration im SCAD-Modell hat. Das In-vivo-Experiment zeigte auch, dass Akr1c18 die Faszien- und Epidermisdicke beeinflussen könnte. Insgesamt zeigte Akr1c18 eine begrenzte Wirkung auf die Narbenbildung, könnte aber eine gewisse Wirkung auf die Zellmigration haben.

# Abstract

Cutaneous wound healing is a complex physiological process. Abnormal skin damage repair such as chronic wounds caused by diabetes, or excessive scar formation places a huge burden on the patient and society. AAV is widely used in biological research and is an ideal tool for human gene therapy. But AAV is rarely used in the research of cutaneous wound repair due to several technical issues.

Here, we identified that sodium butyrate, a histone deacetylase, can greatly enhance the viral transduction of AAV6 serotypes in the wound healing model – SCAD (scar in a dish). We also optimized the transgenic plasmid using 2A self-cleavage peptide instead of the flexible linker, achieving robust co-expression of GFP and our target gene. Using the optimized system, we investigated the function of Akr1c18 in cutaneous wound healing. Akr1c18 is a steroid dehydrogenase and is mainly involved in the progesterone signal pathway. We found that Akr1c18 overexpression could slightly affect the fibroblast migration in the SCAD model and Akr1c18 overexpressed fibroblast have longer cell shape. However, the overall effect of Akr1c18 overexpression in wound healing is limited. Single-cell RNA analysis showed some elevated levels of progesterone response genes in mature wound fibroblast having reduced Akr1c18 expression. Based on the function of Akr1c18 as a progesterone inactivator, reduced expression of Akr1c18 in mature wound fibroblasts may lead to elevated progesterone levels in the skin, leading to increased progesterone responsive gene expression in wound fibroblasts.

# List of figure

Figure 1.1.1 the structure of the AAV genome. ..... 14
Figure 1.1.2 The AAV transduction mechanism ..... 17
Figure 1.1.3 The pipeline of capsid engineering ..... 20
Figure1.1.4 The strategies to package oversized transgene in AAV vector ..... 21
Figure 1.2.1 The structure of human and mouse skin ..... 25
Figure1.2.2 The stage of cutaneous wound healing ..... 27
Figure 1.3 Single-cell mRNA sequencing analysis of wound fibroblast during wound healing ..... 31
Figure 4.1 Histology characterization of SCAD on day 5 ..... 49
Figure 4.2. AAV6-mediated GFP expression in SCADs ..... 51
Figure 4.3 Sodium butyrate boost AAV transfection in the SCAD model ..... 53
Figure4.4.1. Linker mediated co-expression of GFP and Akr1c18 using AAV system. ..... 55
Figure 4.4.2 2A self-cleavage peptide-mediated the co-expression of GFP and target gene ..... 58
Figure 4.5 the overexpression of Akr1c18 in wound healing in the SCAD model. ..... 59
Figure 4.6 Investigate the role of Akr1c18 in wound healing using an excisional wound model ..... 61
Figure 4.7 The single-cell sequencing analysis of the wound fibroblast during wound healing ..... 63

# List of tables

Table1: Culture media, buffers, solutions and reagents ..... 34
Table2**:** Kits and Enzyme ..... 34
Table3**:** Chemical and solution ..... 35
Table 4 : Bacterial strains ..... 36
Table 5. Primers for Infusion cloning ..... 39
Table 6 Primary antibodies used in the project ..... 45
Table7: Secondary antibodies used in the project ..... 45

# Abbreviations

| Abbreviation | Definition |
|---|---|
| **AAV** | Adeno-associated viruses |
| **Akr1c18** | Aldo-keto reductase family 1, member C18 |
| **Ad5** | adenovirus type 5 |
| **ANOVA** | Analysis of variance |
| **BF** | Bright Field |
| **Col3** | Collagen 3 |
| **CO2** | carbon dioxide |
| **DMSO** | Dimethyl sulfoxide |
| **dNTP** | Deoxyadenosine triphosphate |
| **DNA** | deoxyribonucleic acid |
| **DLK** | Delta-like homolog 1 |
| **DMEM** | Dulbecco's Modified Eagle Medium |
| **En1** | Engrailed 1 |
| **ECM** | extracellular matrix |
| **FBS** | Fetal bovine serum |
| **GFP** | green fluorescent |
| **HEK293** | Human Embryonic Kidney Cells 293 |
| **HR** | homologous recombination |
| **IRES** | the internal ribosome entry site |
| **ITR** | Inverted terminal repeats |
| **IdeZ** | IgG-degrading enzyme |
| **IgG** | Immunoglobulin G |
| **LB** | Lysogeny broth |
| **PBS** | Phosphate buffered saline |
| | |

| Abbreviation | Definition |
|---|---|
| **PFA** | paraformaldehyde |
| **PCR** | Polymerase chain reaction |
| **PEG** | polyethylene glycol |
| **RNA** | ribonucleic acid |
| **RT** | Room temperature |

| | |
|---|---|
| **SCAD** | Scar in a dish |
| **ssAAV** | Single-Stranded Adeno-Associated Virus |
| **scRNA** | Single-cell RNA sequencing |
| **scAAV** | Self-complementary adeno-associated virus |
| **TAE** | Tris-acetate EDTA |
| **tSNE** | t-distributed stochastic neighbor embedding |
| **UV** | Ultraviolet |
| **a-SMA** | Alpha-Smooth Muscle Actin |
| **3D** | 3 dimensions |
| | |

# 1 Introduction

## 1.1 Adeno-associated viral vectors

### 1.1.1 The genomic structure of AAV

The discovery of adeno-associated virus (AAV) can be traced back to the mid-1960s (Atchison, Casto, & Hammon, 1965). It was initially thought to be contamination created during the purification of adenoviruses. However, AAV was later identified as a replication-deficient single-stranded DNA virus that requires the help of helper viruses (e.g. adenovirus, herpes simplex virus, poxvirus) for replication and proliferative infection (Hoggan, Blacklow, & Rowe, 1966).

Adeno-associated virus (AAV) belongs to the Microviridae family and is one of the smallest DNA viruses, consisting of an intrinsic single-stranded DNA genome and a protein shell called Capsid (Figure 1). The viral genome of the AAV virus is approximately 4.7 kb with two 145-nucleotide long inverted terminal repeats (ITR) at the ends (Naso, Tomkowicz, Perry, & Strohl, 2017; Z. Wu, H. Yang, & P. Colosi, 2010). The ITR plays a decisive role in virus replication and packaging. There are two open reading frames, Rep and Cap, between the ITRs. The rep gene encodes four regulatory proteins, referred to as Rep78, Rep68, Rep52, and Rep40. The variation is created through the usage of two different promoters – p5 and p19, and alternative splicing. These proteins are involved in the replication of the AAV genome. Under the control of p40 promoter, the cap gene produces

three coat proteins, VP1 (viral protein 1), VP2, and VP3, by using selective splicing and translation initiation. These coat proteins can be assembled into a 60-subunit subspherical protein shell in a 1:1:10 ratio (VP1: VP2: VP3) (Drouin & Agbandje-McKenna, 2013).

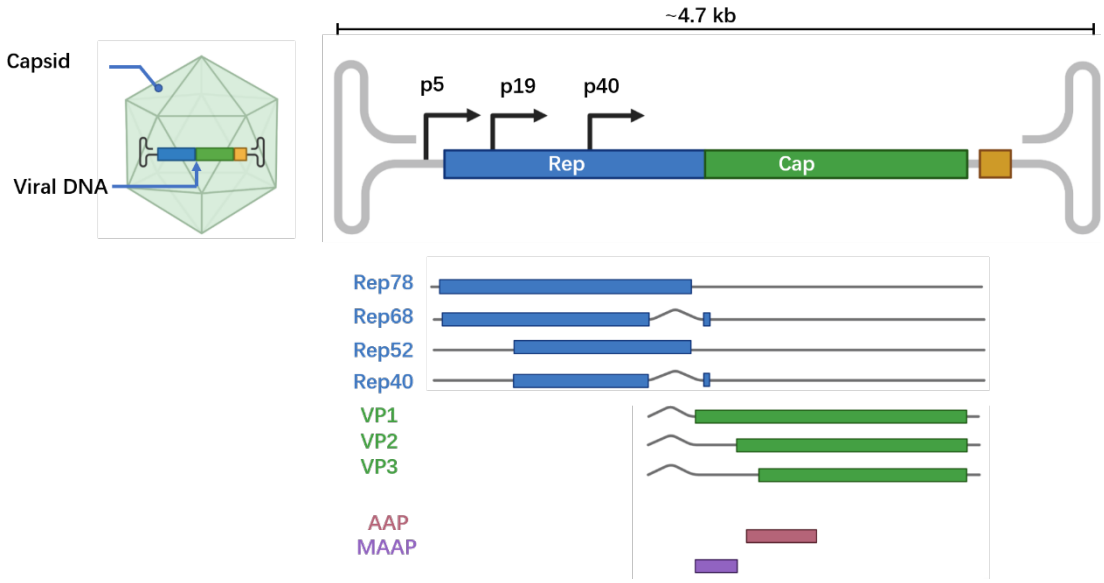


**Figure 1.1.1 the structure of the AAV genome.**

AAV viral particles are composed of an intrinsic single-stranded DNA genome and a coated capsid protein shell. The locations of the three promoters as well as the seven protein-coding regions of AAV have been highlighted in the AAV virus genome.

AAV is widely present in people infected by adenovirus or herpesvirus  o So far, there is no evidence that AAV can cause any disease (Grieger & Samulski, 2005). One of the advantages of using AAV vectors to deliver genes to animals is that AAV vectors produce a much lower immune response compared to other viral vectors (Shirley, de Jong, Terhorst, & Herzog, 2020). Based on these characteristics, recombinant adeno-associated viral systems have been developed to conduct genetic manipulation in animals (Collaco, Cao, & Trempe, 1999). In the AAV delivery system, the transgene is placed between two ITRs, generating the transfer plasmid. The rep and cap genes are integrated into the rep/cap

plasmid. In addition, a helper plasmid containing the adenovirus genes, VA, E2A, and E4, enable the production of high titer AAV. By co-transfecting these three plasmids into HEK293 cells, AAV particles at high concentrations can be obtained, which are suitable for genetic manipulation.

Other viral systems, such as lentiviruses and adenoviruses, are also widely used in biological research. Lentiviruses are mainly single-stranded RNA viruses derived from human immunodeficiency virus (HIV). During transduction, the genome of the lentivirus can be incorporated into the host's genome causing stable transfection. Unlike lentiviruses, adenoviruses are double-stranded DNA viruses that can only mediate transient transfection and the genome of the adenovirus is not integrated into the genome during transfection. The AAV vector is primarily a single-stranded DNA virus. Similar to lentivirus, AAV can mediate long-term transfection of target genes, but its viral genome does not integrate into the host genome. Therefore, AAV is a safe gene vector, but the capacity of AAV is only about 4.7 kb, so it is not suitable for transfection of large fragments of genes.

### 1.1.2 The diagram of the AAV transduction pathway

The transduction of AAV initiates with the binding of the viral particles to the host cell surface receptor, which are usually specific glycans or glycoconjugates displayed on the cell membrane (Nance & Duan, 2015). AAV particles enter cells by numerous endocytic mechanisms, such as clathrin-mediated endocytosis (Bartlett, Wilcher, & Samulski, 2000). After the entry of AAV into the cells, with the help of the endosomal compartments including

the early endosome, late endosome, Golgi, and the perinuclear recycling endosome, the vesicle trapped AAV particles are transported to the perinuclear region through a process called endosomal processing (Nonnenmacher & Weber, 2012). Studies have already shown that endosome processing is closely linked to AAV transduction efficiency (Ding, Zhang, Yan, & Engelhardt, 2005). The direct injection of AAV particles into the cytoplasm results in at least 100 times lower transduction than traditional AAV transduction.

It is generally believed that AAV must exit from the endosome before it is transported into the nucleus in a process termed endosome exit (Ding et al., 2005). In general, only a small proportion of the internalized AAV can enter the nucleus possibly through the nuclear pore. Subsequently, AAV particles in the nucleus undergo uncoating of the capsid shell and release their viral genome. The single-strand DNA of AAV converts into a double-stranded DNA in a replicative form through a second-strand synthesis process (Ferrari, Samulski, Shenk, & Samulski, 1996). The double-strand viral genome begins to transcribe mRNA, which will be exported into the cytoplasm and express the transgene protein.

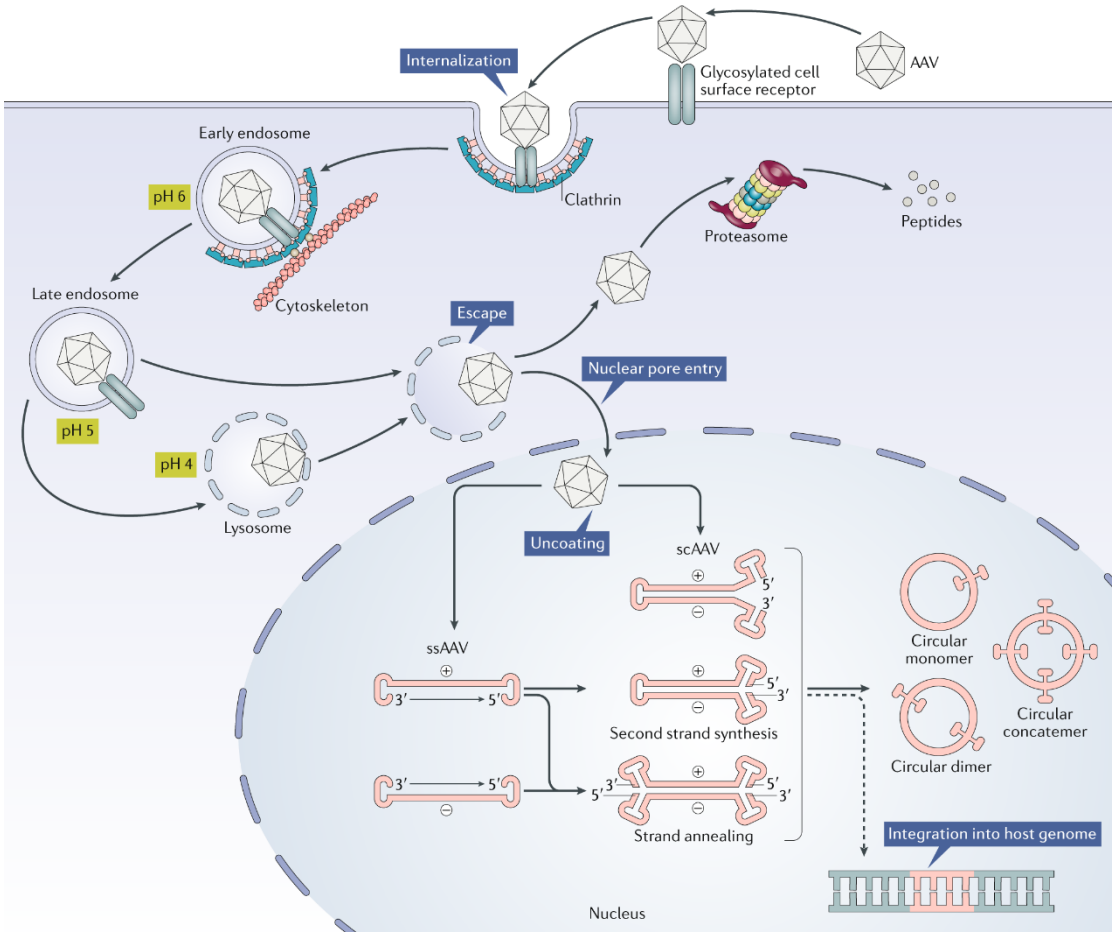


**Figure 1.1.2 The AAV transduction mechanism** (Wang, Tai, & Gao, 2019)

The various steps required for AAV vector transduction include endocytosis of AAV into the host cell, endosomal processing, nuclear entry, and release of single-stranded vector genes, followed by synthesis of second-stranded DNA, which can express viral proteins. A small portion of viral DNA incorporates into the host genome at a low rate.

The wild-type AAV genome is a linear single-stranded DNA (ssDNA), and the conversion to a double-strand from is usually the rate-limiting step for target protein expression. The Self-complementary AAV (scAAV) can bypass this stage and achieves very high transduction efficiency (McCarty, Monahan, & Samulski, 2001). ScAAV is generated by mutating the TRS (terminal resolution site) located in the 3'-ITR, generating the double-strand genome with the single-stranded, inverted repeat genomes at each end and a mutated ITR in the middle. Since only half of the genome can be used, the scAAV is a

suitable vector for small genes. The scAAV vector has more efficient and faster transduction kinetics. It has been shown that the required dose of scAAV in in vivo animal experiments is only 1/20 of the required dose of conventional AAV. Some studies have shown that in animal experiments If scAAV is used, the dose required for in vivo experiments is even 1/20th of that of conventional AAV(Zhang et al., 2020).

### 1.1.3 The AAV serotype and the capsid engineering

Unlike other viral vectors, AAV has different kinds of serotypes. Different AAV serotypes differ in the sequence and the spatial structure of capsid proteins (Z. Wu, Asokan, & Samulski, 2006). In consequence, the cell surface receptors they recognize and bind to differ greatly, leading to the tissue specificity of AAV serotypes. For example, AAV2 has the highest efficiency to transduce kidney cells (Chung et al., 2011); whereas AAV8 has excellent efficiency on hepatocytes (Fang et al., 2018). At least 11 different serotypes have been identified to date. Tissue selectivity of AAV serotypes makes it an ideal gene delivery tool for animal experiments as well as potential gene therapy in humans. However, specificity and efficacy are still issues that hinder the extensively usage of AAV basic and translational researches. One promising strategy is to develop and screen the new capsid, termed as capsid engineering.

Point mutation in the capsid gene is a simple and effective method to increase the stability and specificity of the AAV serotype. A triple AAV6 mutant, AAV6.2FF, containing F129L,

Y445F, and Y731F mutations shows increased lung specificity and robust transgene expression (van Lieshout et al., 2018). Peptide display is another simple approach in capsid engineering that can greatly enhance the interaction between capsid and host cells (Müller et al., 2003). DNA Shuffling is a powerful tool to generate a chimeric capsid library via homology-driven DNA recombination.

A good example of DNA shuffling is AAV-DJ, a chimera of AAV-2, 8, and 9, which shows good transfection in a wide range of cell types and can evade immune neutralization (Grimm et al., 2008). Chemical modification is also a commonly used technique for capsid engineering. In 1999, O'Riordan et al found coupling PEG to the surface of the AAV particles can protect them from neutralizing antibodies in vivo (Lee, Maheshri, Kaspar, & Schaffer, 2005). Capsid engineering can generate a very huge capsid library, which will take a lot of time and effort to screen the aimed capsid. The introduction of DNA barcode and the next generation sequencing technology to capsid engineering have made high-throughput screening possible. One barcode is specifically assigned to one capsid variant. When a capsid library is injected into the animal, different organs are taken for next-generation sequencing, which is able to reveal the viral genome identity and serotype (Jonas Weinmann et al., 2020). In this way, the target capsid can be identified in a fast and efficient way.

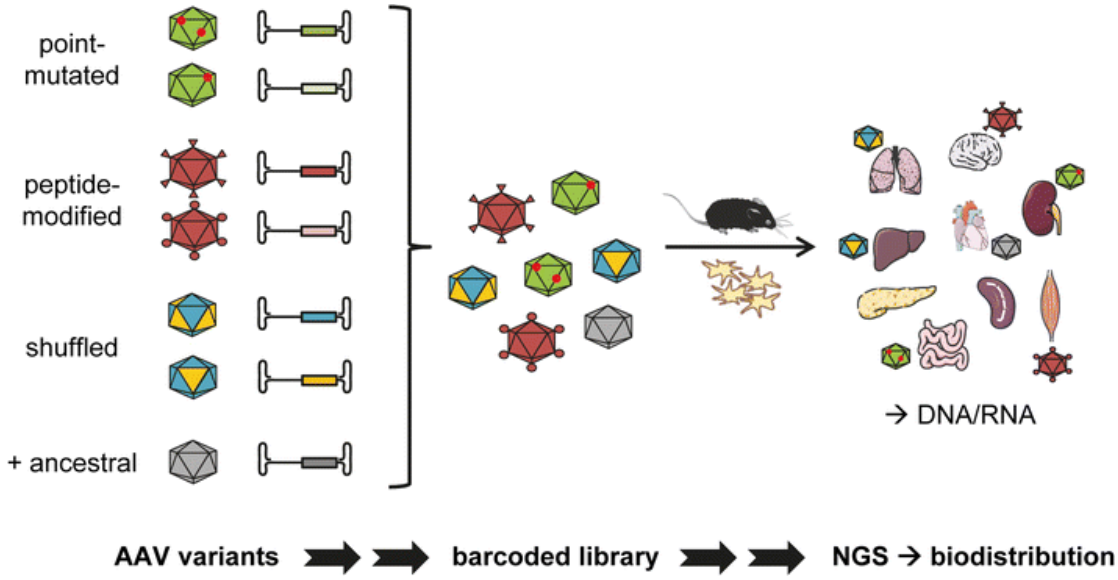


**Figure 1.1.3 The pipeline of capsid engineering** (J. Weinmann & Grimm, 2017)
Capsid engineering begins with the generation of a large library of AAV variants. A barcode is specifically assigned to a capsid variant, forming a barcode library so that each capsid is designated. the AAV library can be administered to animals. With the help of DNA sequencing, it is possible to screen for capsid variants that specifically target certain tissues.

### 1.1.4 The main challenge of AAV in the application of gene therapy

A major limitation of the wide use of AAV is that it has a relatively small packing capacity of about 4.7 kb (Zhijian Wu, Hongyan Yang, & Peter Colosi, 2010), and some important regulatory DNA sequences such as promoters, polyA signal, Woodchuck Hepatitis Virus (WHP) Posttranscriptional Regulatory Element (WPRE) etc, must occupy a considerable amount of packing capacity. Thus, the maximum insertion capacity of ssAAV is about 2.3 kb in most cases, while for scAAV it is only about 1.2 kb (Wu et al., 2007). This makes it very difficult to package larger genes such as Cas9 into AAV vectors, thus limiting the widespread use of AAV in gene therapy.

Split vector approaches can greatly increase the size of the gene delivered by simply

dividing the large transgene into smaller ones. Following transduction, the individual fragments can reassemble and form the full length of the target transgene, which is oversized for a single AAV construct. The overlap strategy is a commonly used split vector approach, which requires an overlap region between the split transgene vectors. It has been shown that during the transduction, the overlap region can facilitate the homologous recombination (HR) between the fragments and reconstitute the full functional transgene (Pryadkina et al., 2015). Trans-splicing strategy can also be used when designing the split vectors. One split vector contains the 5'-fragment of the transgene and splice site donor. The other contains the splice site acceptor and 3'-fragment of the transgene. RNA trans-splicing can reconstruct the full length of the transgene. (Xu et al., 2004). A hybrid strategy is the approach that combines trans-splicing and overlap strategies (Ghosh, Yue, Lai, & Duan, 2008).

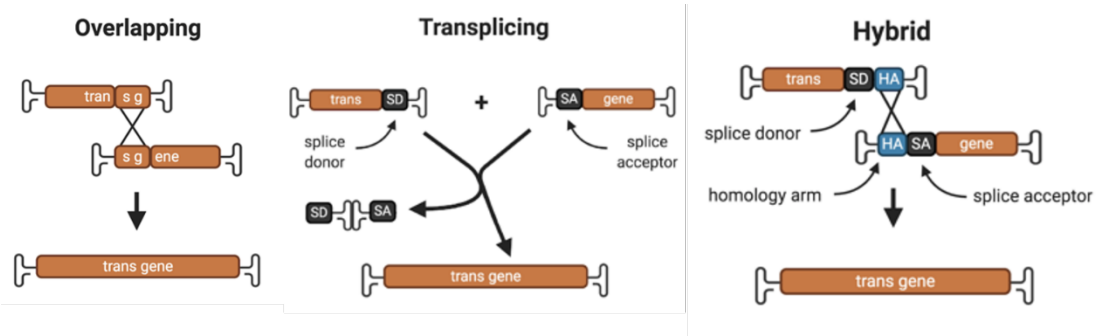


**Figure1.1.4 The strategies to package oversized transgene in AAV vector (Colella, Ronzitti, & Mingozzi, 2018).**

Another issue that affects the widespread use of AAV is that the neutralizing antibodies produced by the immune response inhibit the AAV-mediated gene therapy. Neutralizing antibodies can bind to the AAV envelope proteins, thereby blocking the interaction of AAV

with target cells and preventing AAV from entering the host cell (Mingozzi & High, 2013). In addition to that, the binding of neutralizing antibodies to AAV particles is likely to promote the uptake of viral particles by some phagocytes, such as macrophages. The solutions to reducing neutralizing antibodies in peripheral blood include immunosuppression and plasmapheresis, as well as Capsid engineering. Several studies have recently shown that the administration of an IgG-degrading enzyme (IdeZ) protects AAV particles from the immune system in an animal study (Elmore, Oh, Simon, Fanous, & Asokan, 2020). IdeZ cleaves serum IgG antibodies into Fc and F(ab')2, thereby protecting viral particles from neutralizing antibodies. Because of the ease of use of IdeS, it has been clinically tested in patients with pre-existing IgG against AAV to treat several genetic disorders.

### 1.1.5 The application of AAV vector for in vitro gene transfer

The AAV vectors are rarely used in in vitro experiments. Firstly, transduction mediated by AAV viruses takes a relatively long time to express the target protein. AAV is a single-stranded DNA virus that requires the synthesis of a second strand before the target gene can be expressed. Although this step can be overcome by the use of scAAV viral vectors, the smaller capacity of scAAV vectors, only about 1.2 kb, limits their widespread use. Secondly, the production and purification of AAV are very time-consuming and laborious. In contrast, other viral vectors are much more economical and have very good transfection efficiency in vitro. Despite these limitations, the use and optimization of AAV for in vitro applications have several key advantages over other systems. Firstly, AAV has a target specificity not found in other viral vectors; when infecting transplanted tissue, it only infects

the target cells, not all of them, improving the specificity of the experiment. In addition, AAV can infect dividing and quiescent cells and is relatively safe, thus being allowed to work in the s1 laboratory, whereas other viral vectors such as lentivirus are not.

## 1.2 Wound healing

### 1.2.1. The anatomy and functions of the skin

The skin is the largest organ of the human body. Histologically, the skin can be divided into the epidermis, dermis, and subcutaneous tissue (Yousef, Alhajj, & Sharma, 2022). The epidermis is the outermost layer of the skin. The cell types in the epidermis are keratinocytes, melanocytes, Langerhans cells, Merkel cells, and other immune cells. Keratinocytes are the main cell constituents of the epidermis, and account for more than 90% of the epidermal cells. Melanocytes distributed in the keratinocytes can produce melanin to defend against UV damage. Langerhans cells belong to the monocyte-macrophage system, equipped with innate immune cell function including phagocytosis, antigen recognition and processing (Fore, 2006).

The dermis lies beneath the epidermis and is separated by the basement membrane, which is a thin, flexible, sheet-like extracellular structure. Large portion of blood and lymphatic vessels, and peripheral nerves are embedded in the skin fascia. Most of the dermal cells are fibroblasts, while macrophages and mast cells can also be found in the dermis (Yousef et al., 2022). The dermis can be divided into the papillary dermis and the reticular dermis. The papillary dermis contains loosely arranged collagen fibers, nerve

endings that sense touch, pain, and temperature, and small blood vessels - capillaries - that supply oxygen and nutrients to hair follicles and epidermal cells. The reticular dermis contains plenty of collagen and elastin, creating a dense layer of connective tissue that can provide skin its strength and elasticity.

The subcutaneous layer is located below the dermis and is the innermost layer of the skin. It is composed of several sub-strata layers including subcutaneous fat, a panniculus carnosus muscle that is abundant in rodents and minimaly present in human skin, and a deep layer of gelatinous connective tissue termed as superficial fascia (Stecco, Macchi, Porzionato, Duparc, & De Caro, 2011). The function of the subcutaneous layer is to support the connection of the skin to the underlying bones and muscles. It contains mainly loose connective tissue and lobular fat, which functions as fat storage and thermal insulation and provides a cushion against external forces on the skin. It also contains blood, lymphatic vessels, and nerves, which are larger than those in the dermis and primarily embedded in the deep fascia layers. The major cell types here are fibroblasts, macrophages, and adipocytes.

-

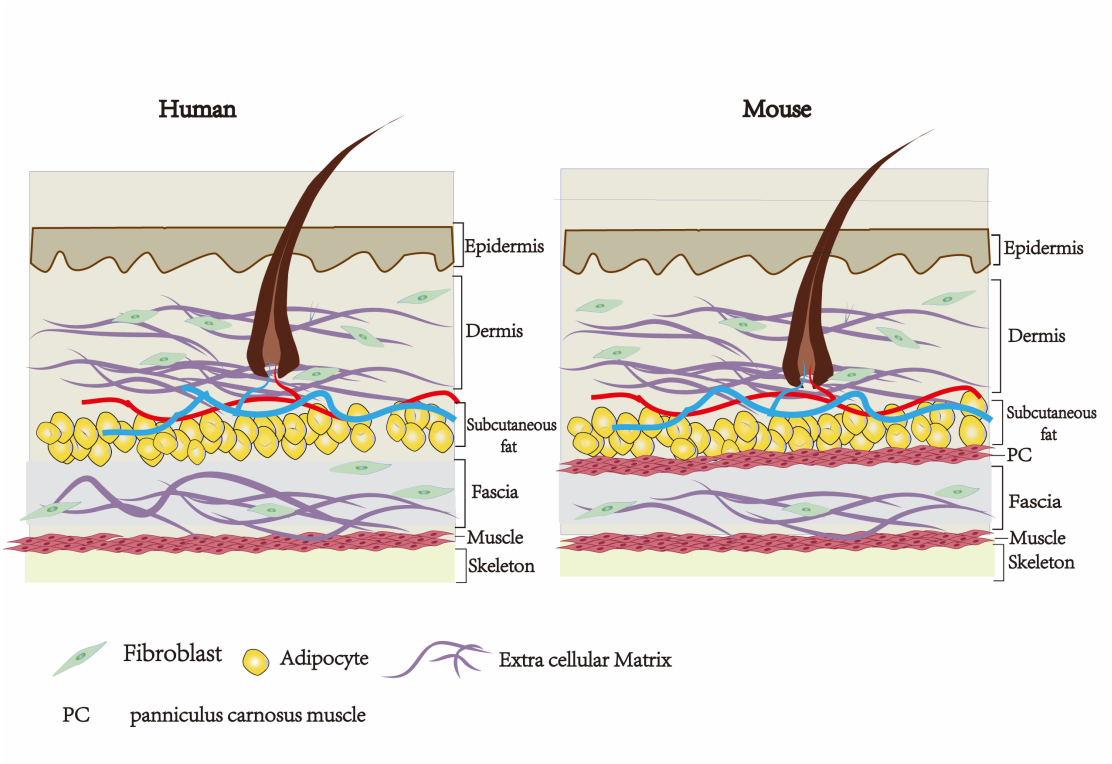


**Figure 1.2.1 The structure of human and mouse skin**

## 1.2.2 The stages of skin wound healing

Skin wound healing can be divided into four phases, hemostasis, inflammation, proliferation, and remolding. Hemostasis occurs immediately after tissue damage, and components of the coagulation cascade are needed to prevent ongoing blood and losses. The vascular endothelium in the blood vessel can sense the damaged vessel and send a signal to the smooth muscle cells within the vessel, which will contract to reduce the loss of blood. Platelets are then activated and change their cell shape from round to spiny, attach to the damaged vessel. Endogenous and exogenous pathways then work together to promote fibrinogen to form a fibrin clot or scab to stop bleeding (ADAMS & BIRD, 2009). When hemostasis has been achieved, histamine is released to increase the permeability of the blood vessels to facilitate the migration of immune cells to the wound site (Rodrigues, Kosaric, Bonham, & Gurtner, 2019)

Subsequently, the inflammatory phase begins wherein neutrophils are firstly recruited to the wound area to remove cellular debris and invading microbes (Hart, 2002). Neutrophils also secrete pro-inflammatory cytokines to recruit other inflammatory cells to the wound area. After a few days, neutrophils experience apoptosis and are engulfed and degraded by arriving macrophages. Macrophage arrival into skin wounds indicates a transition from the inflammation state to a proliferation and remodeling phases (pre-repair phases) of wound repair. Macrophages can secret a cocktail of cytokines and play an important role in wound healing (Ellis, Lin, & Tartar, 2018).

At the proliferation phase, fibroblasts migrate to the wound site, breaking down the fibrin clot and producing the major components of ECM (Xue & Jackson, 2015). For deep wound repair, the latest results from our group suggest that superfascia has an important role in it. Superficial fibroblasts drag the extracellular matrix migrate upward to fill and repair the wound (Correa-Gallegos, 2019). Meanwhile, angiogenesis also begins to provide nutrients and oxygen, promoting the proliferation of fibroblasts and the formation of granulation tissue. Granulation tissue is made up mainly by collagen type 3, fibroblasts, immune cells, and newly formed blood vessels. Subsequently, fibroblasts differentiate into myofibroblasts to contract the wound bed thereby closing open wounds. keratinocytes then proliferate and move towards wound centers to heal the damaged epidermis, in a process termed re-epithelialization. (Nour et al., 2019)

The final phase of wound healing is remolding which starts 2 weeks after injury and continues for a year. During the remodeling phase, the granulation tissue is replaced by scar tissue during which collagen type 3 is replaced by collagen type 1 (Gonzalez, Costa, Andrade, & Medrado, 2016). Myofibroblasts then undergo apoptosis to limit scar production and blood vessels return to the normal homeo

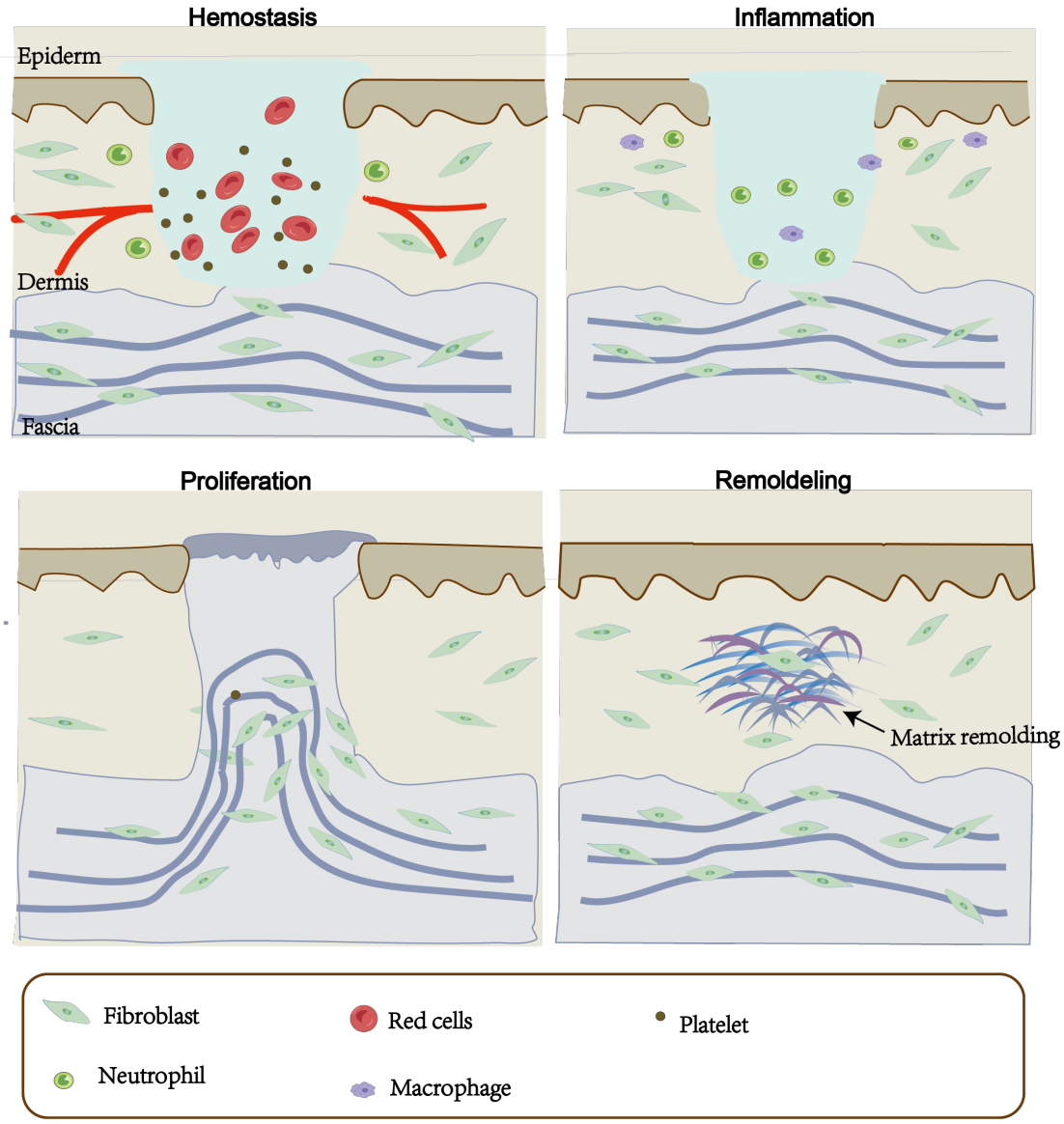


**Figure1.2.2 The stage of cutaneous wound healing**

### 1.2.3 Fibroblast Heterogeneity in Skin Wound Healing

Fibroblasts play a key role in wound healing. With the development of new technologies such as lineage tracing and single-cell RNA sequencing, fibroblasts are no longer considered a single cell entity but a heterogeneous population of functionally and transcriptionally distinct cell types and states. in 2013, Driskell et al. showed that dermal fibroblasts are derived from two separate lineages, namely Blimp1 lineage-derived fibroblasts, which form a papillary dermis that contribute to hair follicle growth, and Dlk lineage-derived fibroblasts, which form the reticular dermis. During the wound repair, fibroblasts derived from the Dlk lineage migrate to the wound site and contribute to wound closure. Fibroblasts of the upper Blimp1 lineage were recruited only during re-epithelialization (Driskell et al., 2013). The above results could explain why follicle regeneration does not occur during wound healing. In 2015, Rinkevich et al. showed two different embryonic fibroblast lineages in the dermis, En1-lineage positive fibroblasts (EPFs), and En1-lineage negative fibroblasts (ENFs). EPFs are primarily responsible for wound scars, suggesting that intrinsic lineage-specific characteristics lead to the fibrotic outcome rather than external stimuli (Rinkevich et al., 2015). During dermal development, a switch occur in the composition of fibroblasts in skin, from an ENF-predominant dermis during early embryogenesis to an EPF-predominant dermis at perinatal stages. The shift in cell composition causes the phenotypic transition from regeneration to scarring seen at perinatal stages of skin development (Jiang et al., 2018).

Fibroblast Heterogeneity can also be caused by cell plasticity during wound healing. Non-

fibroblasts may transdifferentiate into fibroblasts. In 2020, Shook et al. showed that dermal adipocytes near the wound undergo lipolysis and transdifferentiate into ECM-producing myofibroblast (Shook et al., 2020). In 2020, Mithun et al. showed that injury-site myeloid cells give rise to two-thirds of fibroblasts in granulation tissue (Sinha et al., 2018).

## 1.3 The role of Ak1c18 family members and progesterone in wound healing

The traditional view of wound healing is that during skin repair, fibroblasts surrounding the wound migrate into the wound bed where they secrete ECM to form scars and contract the skin (Gurtner, Werner, Barrandon, & Longaker, 2008). In 2019, Our group has shown that the fascia underneath the wound plays a key role in wound repair. Fascia fibroblasts, we found, drag the pre-existing ECM and migrate upwards into the wound bed (Correa-Gallegos et al., 2019). We performed a single-cell RNA sequencing (scRNA-Seq) analysis on skin and wound fibroblasts, and identified a series of genes, showing gradually reduced expression along pseudo time trajectory(). In this series of genes, we selected Akr1c18 as a lead target to investigate in the context of wound healing. Akr1c18 transcripts are highly expressed in the fascia but low expressed in the mature wound fibroblasts, indicating it is essential for initiating the early phases of wound healing (Figure 1.3 D)

Akr1c18 is a hydroxysteroid dehydrogenase, belonging to the Aldo-keto reductase super family (Vergnes, Phan, Stolz, & Reue, 2003). Akr1c18 converts progesterone into 20-alpha-dihydro-progesterone through its reductase activity, thus involved in the progesterone signal pathway. Genetic ablation of Akr1c18 leads to a high level of

progesterone and a delay of parturition in mice (Piekorz, Gingras, Hoffmeyer, Ihle, & Weinstein, 2005). Progesterone is an endogenous sex hormone that is involved in pregnancy maintenance and menstrual cycle regulation (Roberto, 2016). Mechanistically, progesterone and other progestins bind to the progesterone receptor, leading to receptor dimerization, and the receptors translocate to the nucleus to initiate the transcription of progesterone-responsive genes (Wetendorf & DeMayo, 2014).

Progesterone receptors are presented on a variety of innate immune cells (Hall & Klein, 2017). Progesterone administration inhibits the activation of macrophages and dendritic cells in vitro. Progesterone Receptor A/B are also present in cultured human dermal fibroblasts and keratinocytes (Im et al., 2000). Based on the function of Akr1c18 as a progesterone inactivator, Akr1c18 may be able to adjust the availability of circulating progesterone, thus controlling the influence of progesterone on the skin.

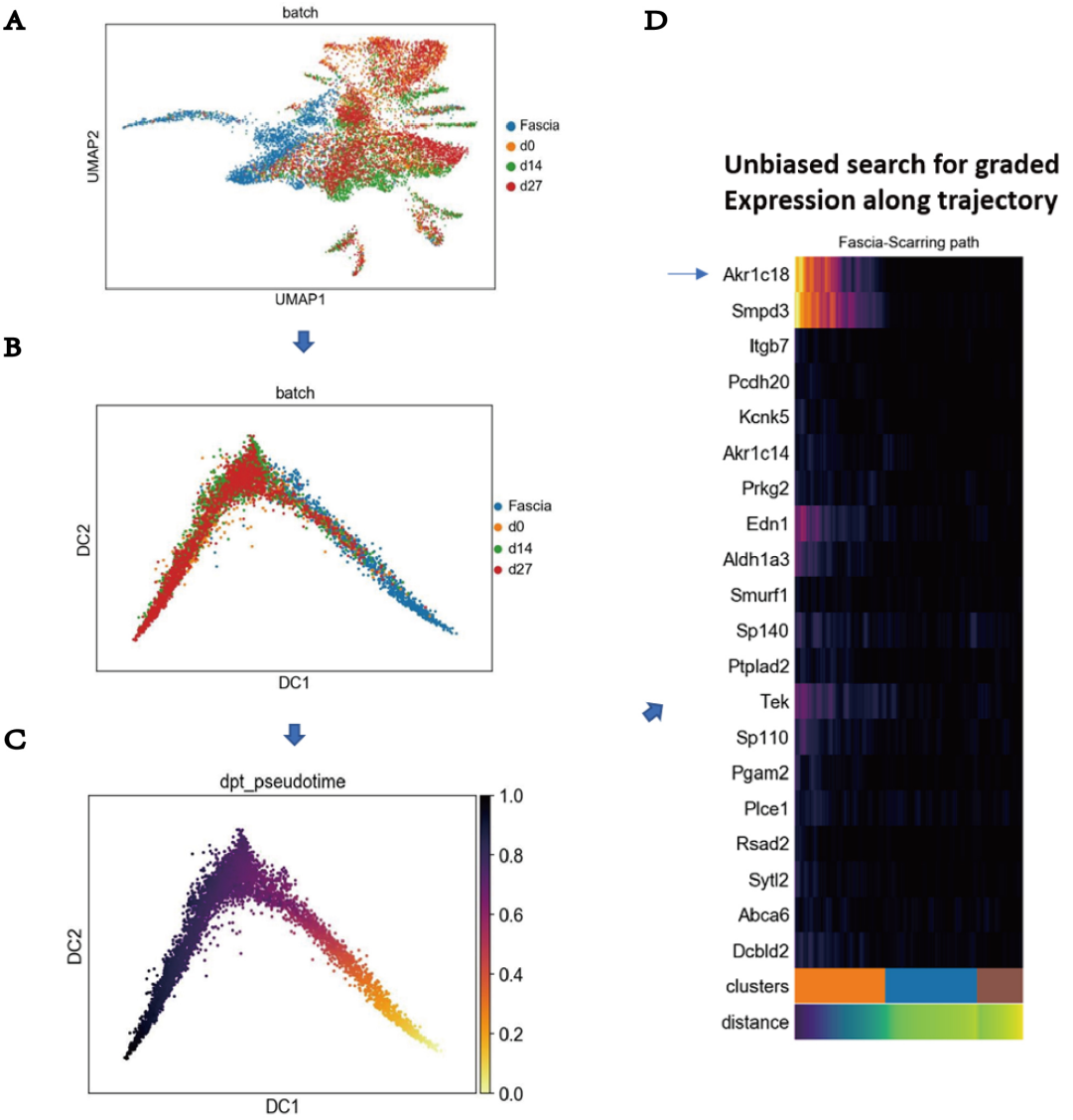


**Figure 1.3 Single-cell mRNA sequencing analysis of wound fibroblast during wound healing**. (A)The UMAP of fascia fibroblasts and wound fibroblasts at days 0, 14, and 27 after wounding. (B) The diffusion maps of fibroblast of fascia fibroblasts and wound fibroblast at day 0, 14, and 27 after wounding. (C) pseudotime trajectory of fascia fibroblasts and wound fibroblast at day 0, 14, and 27 after wounding. (D)Heap map of genes that along the pseudo time trajectory from the fascia to scarring state.

## 1.4 The aim of the thesis

Skin wound healing is a complex physiological process involving the combined involvement of various cells such as immune cells, fibroblasts, and keratinocytes (Singer

& Clark, 1999). Abnormal skin damage repair such as chronic wounds caused by diabetes, or excessive scar formation places a huge burden on patients and the society as a whole (George Broughton, Janis, & Attinger, 2006). The AAV-mediated gene therapy is a promising approach for the treatment of excess scarring or chronic wounds. However, due to the technical issue, the application of AAV on skin is rare.

The first purpose of this thesis is to optimize the AAV system in order to enable efficacious genetic manipulation on an ex vivo wounding/scarring model termed as SCAD (SCAr-in-a-Dish). Although AAV is widely used for gene delivery in animal experiments, the applications of AAV for ex vivo experiments are limited (Lundstrom, 2004). After testing different serotypes, the AAV 6 serotype proved to be effective in the ex vivo SCAD model transfection. However, its efficiency is not good enough. In this project, I have identified a chemical compound, sodium butyrate, which boosts the transfection efficiency of AAV6 in ex vivo SCAD models. I also optimized the transgene plasmid using 2A self-cleavage peptide instead of a flexible linker, achieving robust co-expression of GFP and our target gene. The 2A self-cleaving peptide is a very short peptide (about 20 amino acids) that can induce ribosome skipping during translation. The 2A self-cleaving peptide is often used in genetic engineering to cleave a long peptide into two short peptides.

The second purpose of the thesis is to investigate the functional role of Akr1c18 in wound healing. Akr1c18 is a steroid dehydrogenase that modulates the availability of circulating progesterone and thus might control the magnitude and effects of progesterone on the skin

(Pelletier & Ren, 2004). Akr1c18 shows a dynamic expression pattern along pseudotemporal trajectories during wound healing. But the function of Akr1c18 and progesterone in wound healing have never been investigated. We explore the function of Akr1c18 in skin injury repair in this thesis.

# 2 Experiment materials

## 2.1 Cell lines used in this project

AAVpro® 293T Cell Line (Takara)

## 2.2 laboratory equipment

1. $CO_2$ Incubator (Thermo)
2. Biological safety cabinet (Thermo)
3. Liquid nitrogen tank
4. Stereo Microscopes (Leica)
5. Live-cell imager system
6. Axio imager 2 (Zeiss)
7. THUNDER Imaging Systems (Leica)
8. Confocal microscope LSM 710 (Zeiss)
9. pH meter InoLab pH 720 (WTW)
10. Analytical scales (BEL engineering)
11. Lab shaker (vevor)
12. Magnetic stirrer (Vevor)
13. Metal Bath (Hettich)
14. Micro 200R (Hettich)
15. Plate centrifuge 5430 (Eppendorf)
16. Hettich® ROTANTA 460/460R centrifuge (Hettich)
17. NanoDrop spectrophotometer (Thermo)
18. Thermal Cyclers (Biorad)

19. LightCycler® 480 Instrument
20. Gel Doc XR Imaging System (Biorad)
21. Gel electrophoresis instruments (Biorad)
22. Minus 20-degree refrigerator (Thermo)
23. Minus 80-degree refrigerator (Thermo)
24. Microtome Cryostat (Leica)
25. Autoclave sterilizer (SYSTEC)

## 2.3 Culture media, buffers, solutions and reagents

Table1: Culture media, buffers, solutions and reagents

| Name | Composition |
|---|---|
| SCAD medium | DMEM/F12<br>1% Non-Essential Amino Acid<br>1% penicillin/streptomycin<br>10% FBS<br>1% Glutamine |
| HEK 293T cells Medium | DMEM -high glucose<br>1% sodium butyrate<br>1% penicillin/streptomycin<br>10% FBS<br>1% Glutamine |
| Virus precipitation buffer (5X) | 40% PEG8000<br>2.5M NaCl |
| LB media | Dissolve 25g LB powder in IL distilled water and autoclave. |
| PEI transfection solution | Dissolve 1g of PEI in 1 liter of ultrapure water, and adjust the pH to 7. Aliquot and store in a -80°C freezer. |

## 2.4 Kits and Enzyme

Table2**:** Kits and Enzyme

| Name | Company | Catalog# |
|---|---|---|
| BamH I | Thermo Scientific | FD0054 |
| NotI | Thermo Scientific | FD0593 |
| Xho I | Thermo Scientific | FD0694 |
| EcoR I | Thermo Scientific | FD0274 |
| RNase A | Thermo Scientific | EN0531 |
| Phusion® High-Fidelity PCR Kit | New England Biolabs | E0553S |
| Cryonase™ Cold-Active Nuclease | Takara Bio | 2670A |
| Quick Blunting™ Kit | New England Biolabs | E1201S |
| Q5® High-Fidelity 2X Master Mix | New England Biolabs | M0492S |
| Quick Ligation Kits | New England Biolabs | M2200S |
| NEBuilder® HiFi DNA Assembly Cloning Kit | New England Biolabs | E5520S |

| | | |
|---|---|---|
| Quick Ligation Kits | New England Biolabs | M2200S |
| Monarch® PCR & DNA Cleanup Kit (5 µg) | New England Biolabs | T1030S |
| Monarch® Plasmid Miniprep Kit | New England Biolabs | T1030S |
| PureLink™ HiPure Plasmid Filter Maxiprep Kit | Thermo Scientific | K210016 |

## 2.5 Chemical and solution

Table3**:** Chemical and solution

| **Name** | **Company** | **Catalog#** |
|---|---|---|
| Sodium butyrate | Sigma-Aldrich | B5887-1G |
| PEG8000 | Sigma-Aldrich | 89510-250G-F |
| Acetic acid | Sigma-Aldrich | A6283-1L |
| Agarose | Sigma-Aldrich | A9414-100G |
| Ampicillin | Roth - Carl Roth | K029.5 |
| HEPES | Sigma-Aldrich | H0887-100ML |
| Isopropanol | Roth - Carl Roth | 9781.1 |
| TWEEN®20 | Biorad Laboratories | 1610781 |
| Sucrose | Sigma-Aldrich | 84097-1KG |
| Sodium chloride (NaCl) | PanReac Applichem | APP A2942,5000 |
| Glycerol | Sigma-Aldrich | G5516-100ML |
| LB medium powder | Roth - Carl Roth | X968.2 |
| PFA 16% | VWR International | 43368.9M |
| CHLOROFORM | Sigma-Aldrich | C2432-1L |
| β-Mercaptoethanol (β-ME) | PanReac Applichem | APP A1108,0100 |
| BSA | Sigma-Aldrich | A4503 |
| GeneRuler DNA ladder | Thermo Fisher Scientific | SM0311 |
| Media Growth Medium, agar, ampicillin | LIFE Technologies | Q60120 |
| Tris | Applichem | A1379,5000 |
| Methanol | Roth - Carl Roth | P717.1 |
| AAVpro® Extraction Solution | Takara | 6235 |
| Dimethyl sulfoxide (DMSO) | Santa Cruz | sc-358801 |
| EDTA | Sigma-Aldrich | 01-862-1B |
| DISPASE II | Sigma-Aldrich | D4693-1G |
| 50X TAE buffer | Roth - Carl Roth | CL86.1 |

## 2.6 Laboratory animals

The Adipo$^{Cre}$, TM4 and C57BL/6J strains were purchased from the Jackson Laboratory

and housed at the Helmholtz center animal facility. Adipo$^{Cre}$ transgenic mice were crossed with TM4 reporter mice. The P0 and P1 pups from Adipo$^{Cre}$; TM4 and C57BL/6J mice were used for the SCAD experiments. The animal room is maintained at constant temperature and humidity with a 12-h light cycle. All animal experiments were approved by the Government of Upper Bavaria and registered under the project ROB-55.2-2532.Vet_02-16-61. This study complies with all relevant ethical regulations regarding animal research.

## 2.7 Bacterial strains

Table 4 : Bacterial strains

| Name | Vendor | Catalog# |
|---|---|---|
| 5-alpha Competent E.coli | New England Biolabs | C2987H |
| NEB® Stable Competent E. coli | New England Biolabs | 18258012 |
| One Shot™ Stbl3™ Chemically Competent E. coli | Thermo Fisher Scientific | C737303 |

# 3. Methods

## 3.1 The design of cloning primers.

The cloning primers were designed based on the coding DNA sequence (CDS) of Akr1c18. The Kozak sequence was included in the 5'-end of forward primers to help the translation of eukaryotic genes. To facilitate the ligation of Akr1c18 to the AAV overexpression vector, restriction sites were added to the 5'-end of forward and reverse primers. The Akr1c18 CDS was amplified using the Phusion™ High-Fidelity DNA Polymerase (Thermo Scientific). The plasmid template was purchased from the

original Akr1c18 subcloning vector. The forward primer is 5’ -GGA TCC ACC GGT CGC CAC CAT GAA TTC CAA AAT TCA GAA- 3’. The reversive primer is 5’ -CTC CTC GAG ATA TTC ATC GAA GAA TGG AA- 3’

## 3.2 Restriction digestion reaction

Approximately 2 μg of vector plasmid or PCR product was incubated with restriction endonucleases for 1 hour at 37°C. Reactions were terminated by the addition of 1ul EDTA (100mM). The digestion efficiency was then checked by DNA electrophoresis. The total amount of enzyme should not exceed 1/10 of the reaction volume to reduce star activity (i.e., the enzyme cut a sequence which is only similar, but not identical to their defined recognition sequence). The incubation time was determined by the activity of the enzyme.

## 3.3 Ligation reaction

The vector backbone and the target gene fragment should be cleaved with the same restriction endonuclease to generate the same sticky ends. About 50 ng PCR products were combined with 50 ng linear vector, 1 uL ligation buffer, and 1uL T4 DNA ligase, filled up to 10 uL with nuclease-free water. The mixture was incubated at 16 °C overnight. A molar ratio of 1/3-1/10 of vector backbone to target gene fragment in the ligation reaction is adopted.

## 3.4 Transformation

Competent DH5α or NEB® Stable *E.coli* cells were thawed on ice. Approximately 3 uL of ligation product was added to 50 uL of competent cells and placed on ice for 30 minutes. The mixture was then heat-shocked in a 42°C water bath for 90 seconds to allow the plasmid to enter bacteria and then the mixture was quickly placed on ice for 2-5 minutes. The mixture was then plated onto LB plates with 100 μg/ml ampicillin and incubated at 37°C overnight. If the plate was kana resistant, it was necessary to activate the bacteria before plating.

## 3.5 Infusion cloning

Infusion cloning is a novel method of vector construction. This method allows the introduction of multiple gene fragments at one time based on homologous recombination. This method is particularly useful and suitable for multi-fragments cloning.

First, vectors were linearized by restriction digestion or by PCR amplification. Primers for the multiple introduced fragments were designed by SnapGene software, and amplified by high-fidelity DNA polymerase. An overlap of 15-20 bp among the introduced fragments, and an overlap of approximately 20 bp between the fragments and the vector backbone were designed, to ensure a proper infusion. The introduced fragments also need to have with the vector backbone.

In a 10 uL recombination reaction, the linear vector and multiple fragments were mixed with a 2X recombinant master mix. Subsequently, the mixture was incubated at 50°C for 15 minutes. The transformation was performed using the protocol described above. Colony PCR or restriction digestion was used to identify the correct colonies. Sequencing was performed for the further confirmation.

Table 5. Primers for Infusion cloning

| | Sequences (5'→3') | |
|---|---|---|
| Akr1c18 | Forward | GTTTAGTGGATATCCTTAAGGGATCCACCGGTCGCCAC |
| | Reverse | CTCTGCCCTCCTCGAGATATTCATCGAAGAATGG |
| GFP | Forward | GAGGTTGATTTTAGAATTCCTTGTACAGCTCGTCC |
| | Reverse | ATATCTCGAGGAGGGCAGAGGAAGTCTGC |
| WPRE | Forward | GGAATTCTAAAATCAACCTCTGGATTACAA |
| | Reverse | AGGGATGCCACCCGTGGATCGCGGGGAGGCGGCCCAAA |

## 3.6 AAV production and purification

AAV production was based on the helper-free AAV system provided by Takara, which did not require the use of helper viruses. To prepare viral particles, HEK 293 cells were co-transfected with transgene plasmid, pRC, and pHelper using the PEI-mediated transfection method. 12-16 h later, the medium was replaced with a starvation medium containing 2% FBS. AAV particles were harvested 3 days after transfection. HEK 293cells were scraped with a cell spreader and the cell suspension was centrifuged to form pellets.

To harvest AAV particles from the supernatant medium, the medium was collected and

mixed with 50% PEG8000 solution and 5M NaCl solution to obtain a final concentration of 10 % PEG and 0.5M NaCl, respectively. The mixture was then incubated on ice overnight to precipitate the virus. The virus particles were resuspended in 10 mL of 25 mM HEPES buffer. Intracellular viral particles were extracted from collected HEK cell pellets. Approximately 10 ml of AAV extraction A buffer (Takara) was used to lyse cell pellets from 5 T225 flasks. The mixture was incubated at RT for 10 min and centrifuged at maximum speed and the supernatant was collected. 1ml of Extraction Solution B (Takara) was added and mixed well to further lyse the cell pellet. Then 500 ul of Cryonase™ was added and incubated at 37°C for 30min to remove contaminated DNA or RNA. After centrifugation at maximal speed for 10 min, the supernatant was collected, which contained the intracellular AAV virus. The intracellular AAV virus particles were combined with the extracellular AAV virus particles in the medium and transferred to a 15ml Amicon Ultracentrifuge filter at 100 kDa. The mixture was spined and discarded the flow-through fraction. 5 ml of PBS was added 3 times to desalinate the virus particles. The purified virus particles were aliquoted and stored at -80°C for long-term storage.

## 3.7 Virus titration

The number of genome-containing particles was determined by qPCR. The positive control was a plasmid stock of $2x10^9$ molecules / μL and the positive control is diluted to create a standard curve. qPCR reactions were performed using 2× SYBR Green qPCR mixture combined with 10nM forward primers, 10nM reverse primers, and 2 μl of template DNA or diluted positive control in a final volume of 10 μl. The PCR

conditions started with a denaturation step at 95°C for 2 minutes, followed by 35 cycles of denaturation at 95°C for 5 seconds, annealing and extension at 60°C for 30 seconds, and followed by a final stage of the melting curve phase. The viral titer of samples (viral genomes (VG)/mL) was calculated based on the standard curve and sample dilutions.

## 3.8 Realtime PCR

### 3.8.1 Extraction of cellular RNA (6-well plate)

Cells are digested with 0.05% trypsin and collected by centrifugation. Add 1 ml of Trizol to the cell pellet to lyse the cells and release its mRNA. Then add 0.2 ml of chloroform and mix thoroughly. Let the mixture stand at RT for 5 min. After centrifugation at maximum speed, three separate layers appear. The upper layer is the RNA dissolved in the aqueous phase, the middle layer is the protein, and the lower layer is the phenol/chloroform layer. The upper liquid layer is transferred to a new EP tube. An equal volume of isopropanol is added to precipitate the RNA. After centrifugation of the above mixture, the RNA pellet will appear at the bottom of the EP tube. The supernatant is then discarded and 70% ethanol is added to remove salt ions. Place the EP tube in a fume hood for 5-10 minutes to evaporate the ethanol, then add about 30 ul of nuclease-free water to resuspend the RNA and measure its concentration with a nucleic acid quantifier.

### 3.8.2 Reverse transcription

Reverse transcription of cDNA was performed with Verso Reverse Transcriptase from

thermal. Reverse transcription started at 50°C for 50 minutes, followed by 85°C for 5min, based on the instructional manual.

## 3.9 Full-thickness excisional wound model in mice

The 8-10 weeks old C57B6J wild-type mice were anesthetized with medetomidine at 500 μg/kg, midazolam at 5mg/kg, and fentanyl at 50 μg/kg. Under analgesia, two full-thickness excisional wounds were generated with a 5 mm diameter biological punch (Stiefel). Wounds were harvested on days 0, 7, and 14 after surgery, washed with PBS, and then fixed with 4% PFA overnight at 4°C. After being rinsed three times with PBS, wounds were sliced in half and embedded in OCT, then subjected to cryosections and histological stainings.

AAV vectors were subcutaneously injected into the back skin of the newborn pups ( 2 x $10^{10}$ viral genome per mice). Virus transfection efficiency was assessed under a fluorescent microscope on day 3, and a wound was produced in the center of the back skin with a 2-mm punch. Samples were collected on day 7 or 14 after injury.

## 3.10 Scar-in-a-dish (SCAD) assay

The C57BL6/J neonates at P0 or P1 were decapitated with scissors. The dorsal skin was carefully torn off with surgical scissors and forceps. The skin was washed twice with PBS, sampled with a 2-mm biopsy punches, and transferred to a 96-well plate for incubation.  The medium comprised 10% FBS (Life Technologies), 1% GlutaMax

(Thermo Fisher), 1% penicillin/streptomycin (Thermo Fisher), and 1% MEM non-essential amino acids (Thermo Fisher) (Thermo Fisher). The medium per well was changed every other day (about 100ul media per well). And on the fifth day, samples were taken, washed three times with PBS, and used in subsequent histology investigations.

## 3.11 Live imaging of cell migration

SCAD assays were prepared as described above. AAV6 constructs containing target transgenes were added to the media and incubated overnight. To increase the transfection efficiency, the volume of media was reduced to a minimum of 50 ul containing 15 ul purified AAV particles and 20 mM Sodium butyrate (Sigma-Aldrich). Another 50 ul of fresh SCAD medium was added to each well the next day.

On day 4, the sample was embedded in 4% agarose in a 35 mm dish (Corning, 351008). For imaging purpose, the samples were then immersed in a phenol-free DMEM/F-12 medium (Thermo Fisher Scientific, 21041025) containing 10% fetal bovine serum (Thermo Fisher Scientific, 26140079), 1% GlutaMAX (Thermo Fisher Scientific, 35050038), 1% Penicillin/streptomycin (Thermo Fisher Scientific, 15140122), and 1% MEM non-essential amino acids (Thermo Fisher Scientific (Thermo Fisher Scientific, 11140035). Time-lapse imaging was performed with a Leica SP8 MP multiphoton microscope (Leica, Germany) with a modified heating and gas control incubation system (ibidi 10915 & 1192) at 37 °C and 5% CO2. 3D-frames with Z-stacks

were taken every 15 minutes, for 12 hours.

## 3.12 Histology

### 3.12.1 Cryosection

Harvested wound samples were washed three times with PBS and fixed in 4% PFA overnight at 4°C. To prevent the formation of ice crystals during snap freezing, a gradient of 15% and 30% sucrose solutions were used for dehydration. The samples were then embedded in optimal cutting temperature compound (OCT) and snap frozen on dry ice. Cryosections at the thickness of 6-8 um were sliced with a cryostat (NX50, thermal). Slides were stored in a -20°C refrigerator.

### 3.12.2 Immunofluorescence

Frozen sections were thawed and washed three times with PBS to remove the remaining OCT. To facilitate the detection of intracellular proteins, sections were permeabilized with 0.1% triton-x100 for 10 minutes at room temperature (RT). The slides were washed three times with PBS. The non-specific antibody binding was blocked with PBS containing 5% serum from the species that the primary antibody is raised from for one hour at RT. After 1-hour incubation of primary antibody at RT or overnight at 4°C, slides were washed three times with PBST(PBS containing 0.1% Tween20) to remove unbound antibody. The slides were then incubated with the fluorophore-conjugated secondary antibody for one hour at RT and mounted with a DAPI-containing mounting media and analyzed under an inverted fluorescence

microscope (Axio Imager, Carl Zeiss).

Table 6 Primary antibodies used in the project

| Antibodies | Host | Dilution | Company | Catalog | Concentration |
|---|---|---|---|---|---|
| GFP | Chicken | 1/500 | Abcam | ab13970 | 2 ug/ml |
| α-SMA | Rabbit | 1/100 | Abcam | ab5694 | 10 ug/ml |
| Ki67 | Rabbit | 1/200 | Abcam | ab1666 | 5 ug/ml |
| CD31 | Rat | 1/100 | Biolegend | 102421 | 5 ug/ml |
| CD45 | Rat | 1/200 | Biolegend | 103125 | 2.5 ug/ml |
| Tie2 | Rat | 1/50 | Biolegend | 124005 | 10 ug/ml |
| Ter-119 | Rat | 1/200 | Biolegend | 116233 | 1 ug/ml |
| EpCAM | Rat | 1/100 | eBioscience | 48-5791 | 2 ug/ml |
| Akr1c18 | Mouse | 1/100 | Santa Cruz | sc-166297 | 2 ug/ml |

Table7: Secondary antibodies used in the project

| Antibodies | Dilution | Company | Catalog | Concentration |
|---|---|---|---|---|
| Goat anti-Chicken IgY Alexa Fluor® 488 | 1/1000 | Abcam | A32931 | 2 ug/ml |
| Goat Anti-Rabbit IgG Alexa Fluor®594 | 1/1000 | Abcam | A-11012 | 2 ug/ml |
| Goat Anti-Chicken IgG Alexa Fluor®647 | 1/1000 | Abcam | A-21449 | 2 ug/ml |

### 3.12.3 Masson’s Trichrome staining

Cryosections were thawed and fixed with pre-cooled acetone for 10 min. The slides were dried in a fume hood for 5 min before being placed in the preheated Bouin's Solution for 15 min to further fix the sample. Subsequently, the slides were then washed with tap water and placed in Weigert's iron hematoxylin solution for 3 min to stain the cell nuclei. After washing the slides with tap water, the slides were placed in Biebrich Scarlet-Acid Fuchsin solution for 5 min to stain all acidophilic tissue elements.

After washing 3 times with deionized water and the slides were placed in a Phosphomolybdic-Phosphotungstic Acid solution for 5 minutes, followed by being placed in an Aniline Blue solution for 10 minutes to stain the collagen. Then the slides were placed in 1% acetic acid for 2 minutes and rinsed with distilled water. To dehydrate the samples, the slides were put subsequently in 80% and 100% ethanol for 5 min. Finally, slides were cleared with Roti-histol, an organic solvent, and then mounted with Roti®-Histokitt mounting medium.

## 3.13 Statistical analysis

Data were analyzed with the software Graph Prism 9 and the statistical significance was assessed by unpaired two-tailed Student's t-test to compare two groups. The one-way analysis of variance (ANOVA) with Tukey's multiple comparisons was used to analyze multiple comparison procedures. All results are represented as mean ± SEM.

## 3.14 Bioinformatic analysis

### 3.14.1. Sample preparation

wound fibroblasts are isolated from 6-8 weeks mouse. Kill the mice at days 7 and 14 post wounding. Collect the back skin and use a 5mm punch to sample the wound tissue. Chop it into a pulp with scissors. The chopped wound tissue was then placed in DMEM containing Liberase TL (100 μg/mL; Sigma-Aldrich) and DNase I (100 μg/ml; Roche) for 1 h at room temperature for further dissociation. Add 3 volumes of DMEM media containing 10%FBS to stop the dissociation. Pass the above mixture through a 40 um strainer. And pin at 300g for 10 min to get the cell pellets, which will be resuspended in 20% FBS DMEM. Fibroblasts

were isolated via a lineage negative gate (Lin- ) strategy. Incubate the cells with the fluorophore-conjugated CD31 (1:100), CD45 (1:200), Tie2 (1:50), Ter-119 (1:200), and EpCAM (1:100) antibodies. Fibroblasts were isolated by Fluorescence-activated cell sorting (FACS) via a lineage-negative gate. Fascia fibroblast was taken from healthy 6-8 weeks mice. Take out the fascia tissue from the back skin. Then chop the fascia tissue into minces. The following steps are the same. We acknowledge the bioinformatic unit at Helmholtz center performs the single-cell analysis based on the drop-seq strategy. Single-cell cDNA libraries were run on the Illumina HiSeq4000.

### 3.14.2. Bioinformatic process of the single-cell RNA sequencing data

The pre-processing of the single-cell RNA data was performed by the bioinformatic unit at Helmholtz center. Briefly, Trim galore was used to remove adapters and low-quality base calls. Then reads were aligned to the mouse genome (GRCm38.p6 genome) with STAR (version 2.5.2a). We filter the barcode with less than 200 genes. The raw count for each gene was calculated using FeatureCounts. We filtered cells that have >5% mitochondrial counts, or have feature counts more than 2500 or less than 200. We acknowledge Dr. Donovan Correa-Gallegos perform downstream analysis including dimension reduction, clustering, and differential gene analysis with Seurat or Scanpy.

# 4 Results

## 4.1 Characterization of an ex vivo wound healing model termed SCAR in a dish (SCAD).

Skin repair that follows injury is a multifaceted complex process involving the cooperation of fibroblasts, immune cells, and keratinocytes (Gurtner et al., 2008). Wound healing outcomes in animal models are often quite heterogeneous, difficult to interpret, and involve animal ethical issues. To better study the mechanisms of wound repair, many in vitro models have been developed, including monolayer cell cultures, skin grafts, and transwell-mediated co-culture systems (Sami, Heiba, & Abdellatif, 2018). In this project, I used a novel *ex vivo* three-dimensional explant model developed in our laboratory, the SCAr in a dish (SCAD) model (Correa-Gallegos et al., 2019; Jiang et al., 2020).

We excised and incubated 2-mm full-thickness neonatal mouse skin discs that included the epidermis, dermis, panniculus carnosus and subcutaneous fascia, with the fascia side facing upwards (Fig 4.1A). Under these conditions, skin-fascia explants developed uniform scars over a course of 5 days. Compare with other wound model, A significant advantage of SCAD over other in vitro scar models is its ability to observe cell migration in real-time at the single-cell level. Histologic analysis with Masson's trichrome staining revealed masses of fibroblasts that developed increasingly woven connective tissue that bridged between skin folds. The fascia fibroblasts created a plug of collagen fibres that progressively formed scars (Fig 4.1B). Further analysis with immunostaining showed Collagen type 3, a main component of ECM during wound repair, was also highly expressed in SCAD samples, consistent with wound repair in animals (Fig 4.1C).

Myofibroblasts indicated by α-SMA expression can also be seen within the SCAD sample, which play a pivotal role during wound healing and scar formation (Fig 4.1D). Adipocytes were also found to be located in the SCAD sample. Interestingly, we find expression of adipocyte markers such as perilipin, in cells not from adipocyte lineage (Fig 4.1E). One possible reason is that perilipin may not be exclusive to adipocytes alone, or that fibroblasts might experience trans-differentiation into adipocytes.

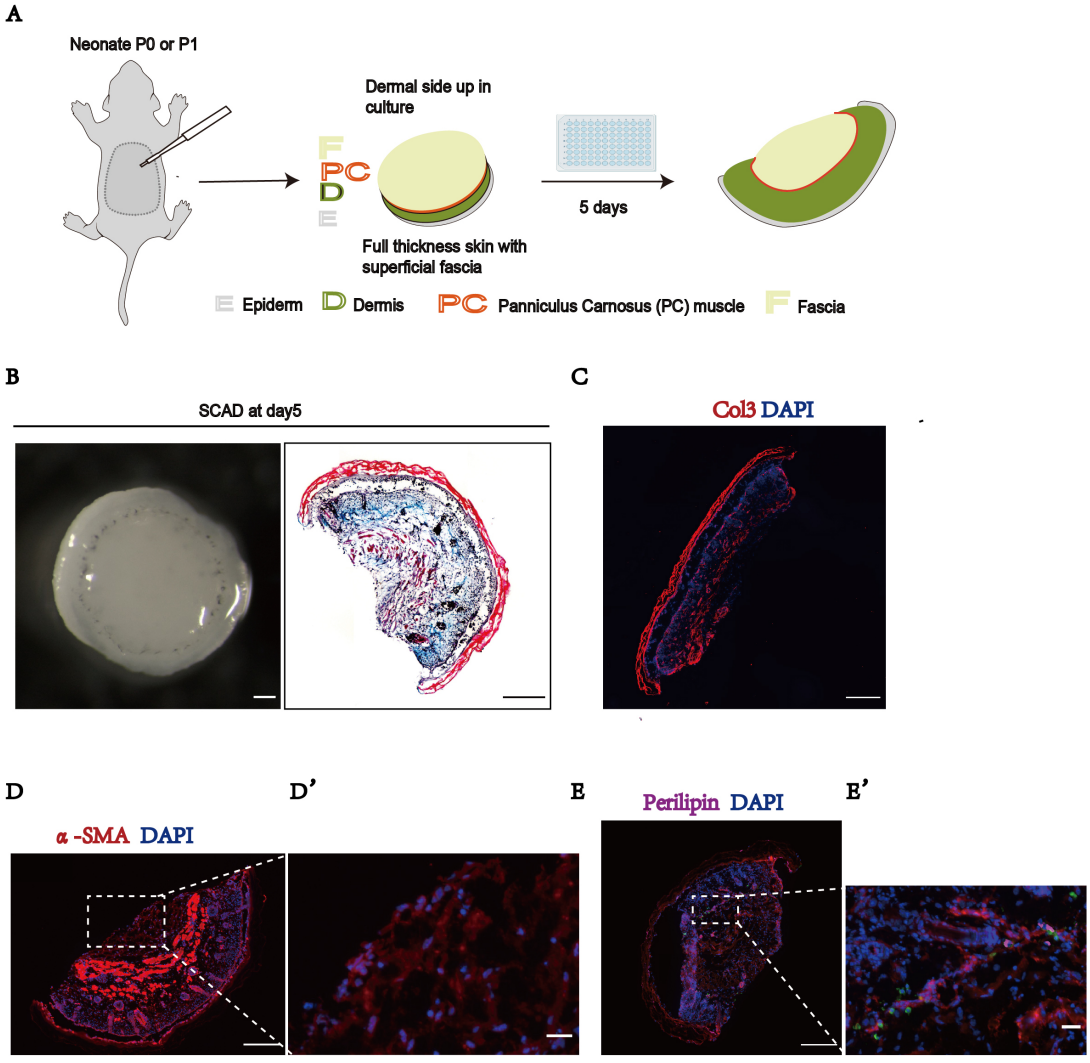


**Figure 4.1 Histology characterization of SCAD on day 5**

(A) The experimental procedure of SCAD model(Scar in a dish). (B) Whole-mount bright-field images (left panel) and Masson's trichrome (right panel) of SCAD sample on day 5. (C) Representative Image of SCAD sample staining with collage3 (red). (D) Representative Image of SCAD sample staining with α–SMA (Red). (E) Representative Image of SCAD sample from Adipoq$^{Cre}$;R26$^{mTmG}$ mice, staining with

perilipin (magenta). The adipocyte (GFP) from adipocyte lineage is located at the bottom left of the enlarged portion. Scar bar B, C, D, E= 200um, D', E' = 25um。

## 4.2 AAV6-mediated transgene overexpression in SCADs

The SCAD model can be used for genetic screening in order to explore the underlying mechanisms of scarring with the advent of identifying advanced treat options for abnormal wound healing. Lentiviruses and retroviruses are ideal tools for gene delivery in vitro. However, the application of these viral vectors is strictly regulated due to biosafety requirements (Baldo, van den Akker, E Bergmans, Lim, & Pauwels, 2013). Therefore, we used AAV vectors, which have lower requirement for safety measurements, and are widely used for animal experiments.

Unlike other viral vectors, AAV has various serotypes, which can target different tissues in vivo. We firstly tested the serotype, AAV-DJ which can successfully transfect many cell lines with more than 10 times higher efficiency than other AAV serotypes. (Westhaus et al., 2020). However, in our result, AAV-DJ was unable to transfect the SCAD, instead the AAV6 serotype is effective in the SCAD transfection (Fig 4.2 A, B). The 3D whole-mount imaging of transfected SCADs revealed strong second harmonic generation (SHG) signals indicative of collagen fibrils, and relatively strong GFP expression (Fig 4.2 C). However, further analysis of the 3D image has shown very few transfected cells in the SCAD tissue (Fig 4.2D). The following histology also confirm that very few cells in SCAD is transfected, which is obviously not enough for any functional analysis (Fig 4.2E). In conclusion, although the AAV6 serotype could transfect SCADs *in vitro*, its efficiency is low. Further

optimization is required.

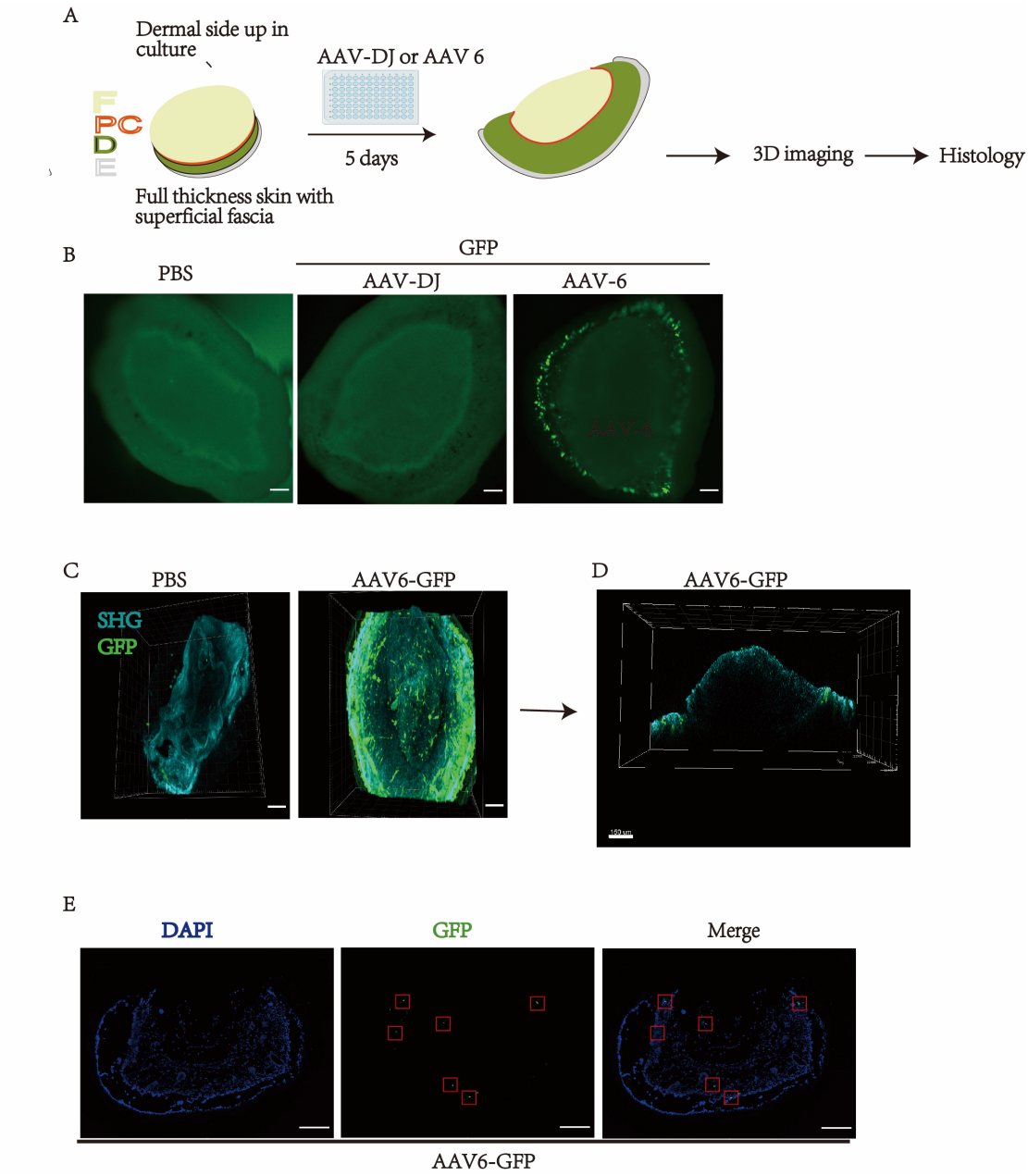


**Figure 4.2. AAV6-mediated GFP expression in SCADs**.

(A) The experiment procedure of AAV-mediated SCAD transfection and analyses. (B) Whole amount image of SCADs transfected with different AAV serotype ($10^{12}$ viral genome per sample) (C) the 3D of SCAD 3 days after transfection with AAV6-GFP. (D) The orthogonal frontal view section of the transfected SCAD on day 3. (E) Histology analysis of GFP expression in the transfected SCAD on day 3, the red box indicates the transfected cells. Scar bar B C, D, E=150 um.

## 4.3 Sodium butyrate is used to boost AAV transfection for in vitro

To improve the viral transfection for SCADs, we tried different experimental approaches. Considering that when retroviruses or lentiviruses are used for in vitro genetic manipulation, small molecule chemical -'polybreme'-need to be added to the media to enhance transgene expression. We hypothesized that it is also necessary to add some small molecule chemical regents to facilitate AAV-mediated in vitro transfection. Several studies have shown that sodium butyrate can facilitate AAV-mediated transfection of in vitro cell lines (Dong et al., 2010). But they never tested it in the ex vivo tissue. In our results, both 3D whole-mount imaging and 2D histological analysis showed that the addition of sodium butyrate resulted in remarkably elevated transfection efficiency, with at least a 20-fold increase (Fig 4.3 A-C). Sodium butyrate is an inhibitor of class I histone deacetylases. To assess whether sodium butyrate administration had side effects on our assay, we examined whether the addition of sodium butyrate affected the second harmonic signal (SHG). The addition of sodium butyrate did not result in an obvious change in the second harmonic signal (Fig 4.3D). In summary, sodium butyrate can greatly facilitate AAV6-mediated infection in the SCAD model.

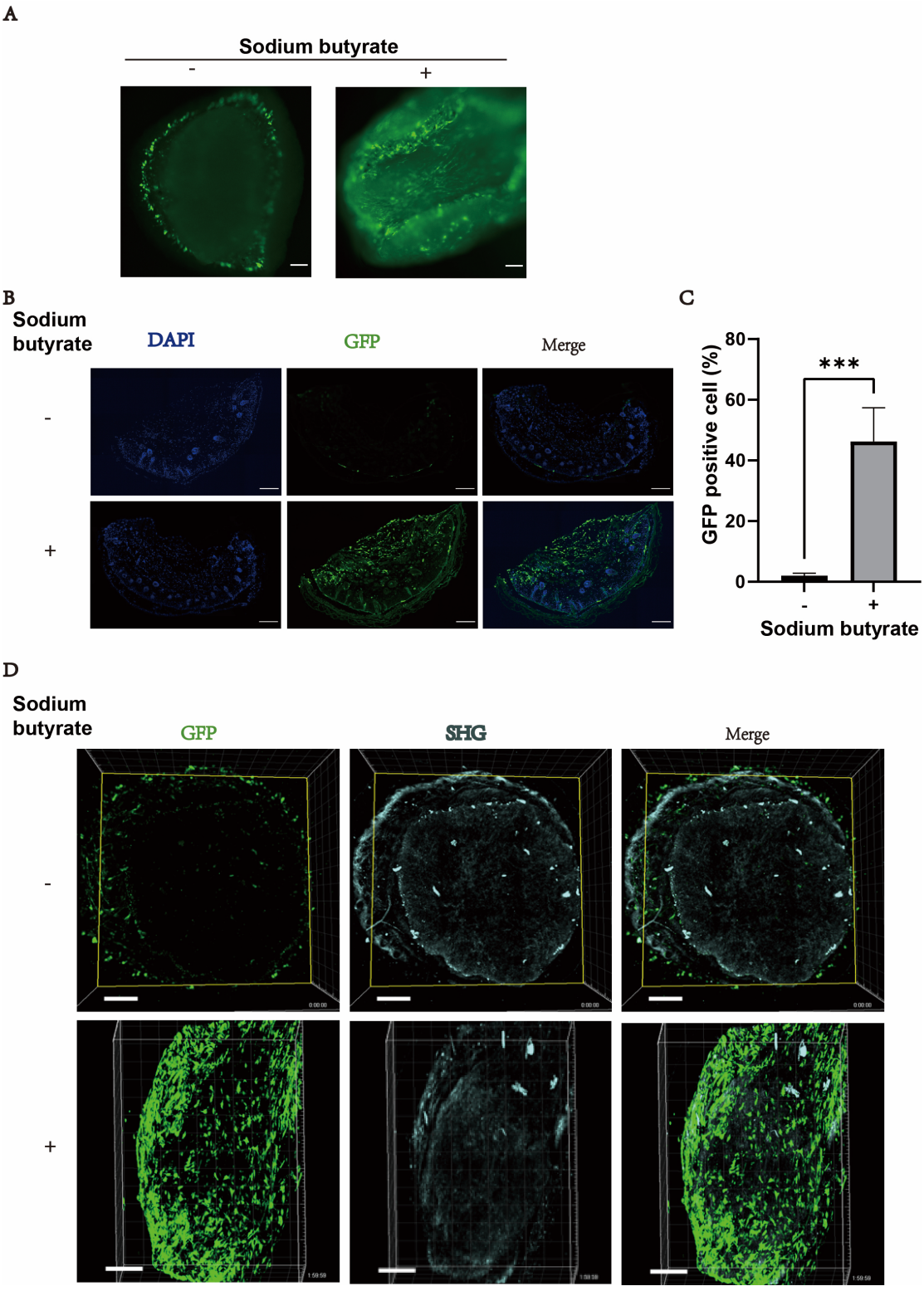


**Figure 4.3 Sodium butyrate boost AAV transfection in the SCAD model**

(A) Whole amount image of SCAD sample transfected with AAV6-GFP with or without 20 mM sodium butyrate (B) Histology analysis of GFP expression in the transfected SCADs with sodium butyrate on day 3 after transfection. (C) Quantification of GFP positive cells in the AAV6-GFP transfected SCAD with and

without sodium butyrate. Mean ± SEM, n=3, p= 0.002, unpaired two-tailed t-test. (D) Whole-mount 3D image of AAV-GFP transfected SCADs with or without sodium butyrate. Scar bar A, B, D = 150 μm.

## 4.4 Design optimization of the AAV transgene construct

### 4.4.1 Linker is not suitable for the co-expression of GFP and target gene using the AAV system.

In order to study the underlying mechanism of wound healing. we performed the single-cell analysis of wound fibroblast. We found Akr1c18 transcripts are highly expressed in the fascia but low expressed in the mature wound fibroblasts, indicating it is essential for initiating the early phases of wound healing (Fig1.3). We created the Akr1c18 fusion GFP overexpression construct overexpression construct which has a flexible linker between Akr1c18 and GFP (Figure 4.4.1A). Compared to SCADs transfected with AAV6-GFP, SCADs transfected with AAV6-Akr1c18-linker-GFP showed very low GFP expression (Fig 4.4.1 B,C). The further histological analysis could not detect any expression of GFP in the fusion protein group (Fig 4. 4.1 D).

Since flexible linker-mediated co-expression strategies have been very successful in some aspects, such as in vivo calcium imaging, this strategy may only be applicable to in vivo gene delivery. Akr1c18 fusion GFP vector may only be suitable for in vivo animal experiments. In order to test the hypothesis, the Akr1c18 overexpression virus particles were injected subcutaneously into newborn pups in the excision wound model (Figure 4.4.1E).However, the GFP expression could not be detected in the fusion protein group in animal experiments (Figure 4.4.1F. G). A possible explanation for this, is that using the

current vector design, i.e., Akr1c18 and GFP formed a fusion protein through a flexible linker. Thereafter, Akr1c18 would very likely affect the structure and stability of GFP, leading to very few GFP-expressing cells detectable. Conversely, the presence of GFP in the fusion protein also probably affects the structure and function of Akr1c18.

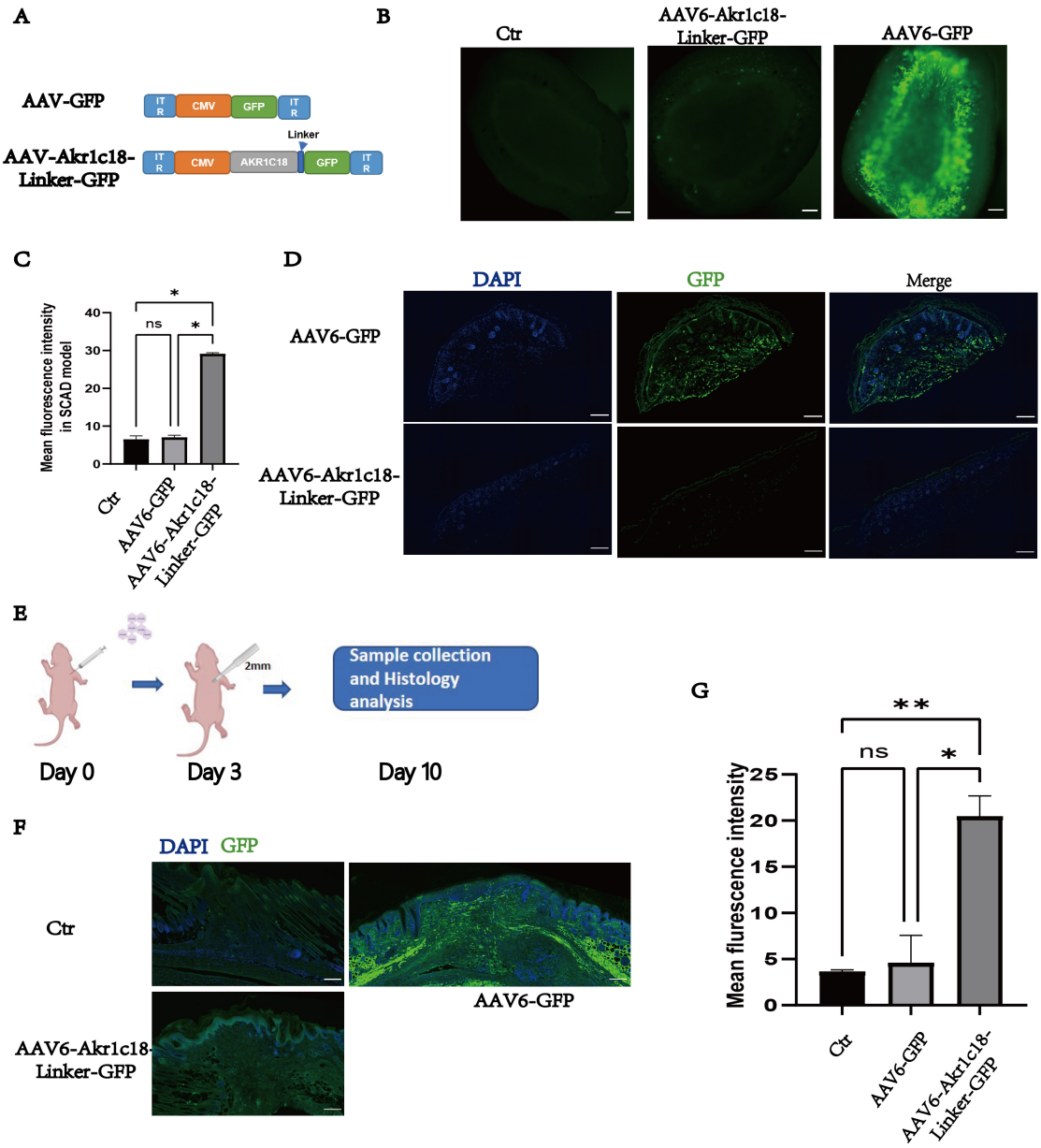


**Figure4.4.1. Linker mediated co-expression of GFP and Akr1c18 using AAV system.**

(A) The map of the AAV overexpression vector. (B)The whole-mount image of SCAD was transfected with AAV on day 3.（C）Quantify the mean fluorescence intensity of GFP expression in SCAD. (D) Histology analysis of GFP in the sample of AAV transfected SCAD. (E)The scheme of AAV mediated gene

manipulation on newborn pups in an excisional wound model. (F) Histology analysis of GFP in the sample of AAV transfected animals. (G) Quantify the mean fluorescence intensity of GFP expression in AAV transfected animals, Mean + SEM, n=3, p= 0.0034, unpaired two-tailed t-test. Scar bar B, D, F = 150 um.

### 4.4.2 2A self-cleavage peptide enables efficient co-expression of GFP and Akr1c18 ex vivo

The 2A self-cleavage peptide strategy is commonly used to achieve the co-expression of multiple genes. The existence of the 2A self-cleavage peptide in the polycistron mRNA can cause ribosomal skipping during mRNA translation, thus producing several independent peptides, without physical linkers. (Figure 4.4.2 A) (Liu et al., 2017). To test this strategy, we constructed an AAV-Akr1c18-T2A-GFP vector containing the 2A self-cleaved peptide between the target gene Akr1c18 and the reporter gene GFP. Transfection of HEK cells with the 2A constructs significantly improved the GFP expression compared with the fusion protein construct (Figure 4.4.2 B, left panel). The internal ribosome entry site (IRES) element is another commonly used strategy for multiple cis-trans expressions. Therefore, we also created an AAV-Akr1c18-IRES-GFP construct. However, it resulted much lower GFP expression level in transfected HEK cells, compared to Akr1c18-T2A-GFP construct (Figure 4.4.2 B, Right panel). Taken together, 2A strategy works best to achieve coexpression of GFP and my target gene.

Next, we applied the AAV6-Akr1c18-T2A-GFP virus for the transfection of SCADs and found it were able to effectively infect the SCAD with very high GFP expression (Figure 4.4.2C). Finally, we used AAV6-Akr1c18-T2A-GFP virus *in vivo* . Wounds were harvested at day 7 post-wounding. The AAV6-Akr1c18-T2A-GFP transduced wounds showed not

only high GFP expression level but also high Akr1c18 expression. Altogether, we have optimized the AAV vectors to enable a robust expression of transgenes to in an ex vivo wound model.

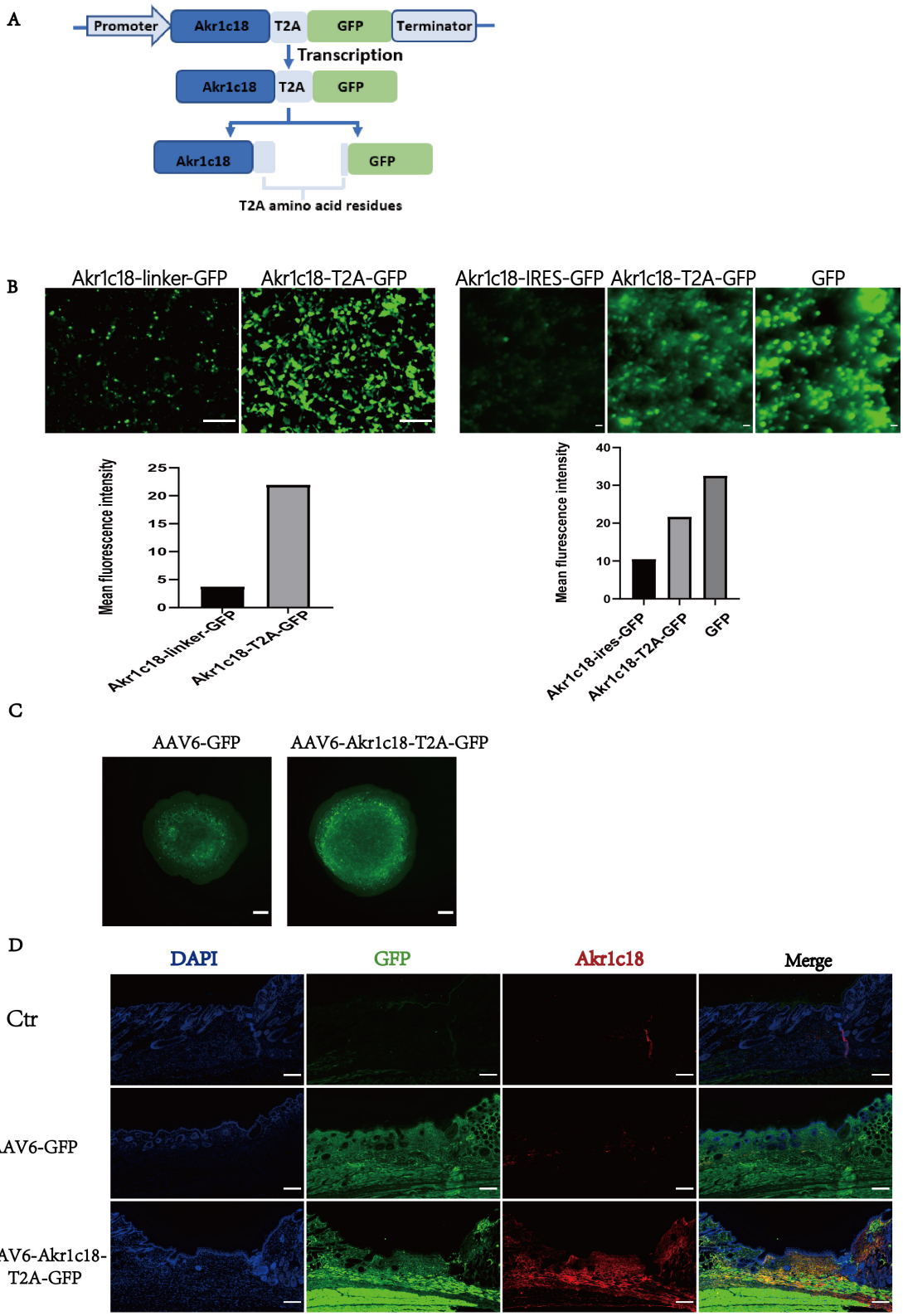

**Figure 4.4.2 2A self-cleavage peptide-mediated the co-expression of GFP and target gene**

(A) The mechanistic diagram of the 2A self-cleavage peptide mediated the co-expression of GFP and the target gene, Akr1c18. (B) The representative images of HEK cells transfected with 2 ug plasmid coding Akr1c18 fusion GFP or Akr1c18-T2A-GFP or IRES-GFP. The quantification seen in bellow. (C) The whole-mount images of SCAD transfected with AAV particles coding GFP or Akr1c18-T2A-GFP. (D) Histology analysis of GFP in the sample of AAV transfected animals. Scar bar B, C, D=150 um.

## 4.5 Investigate the role of Akr1c18 in wound healing in the SCAD model

To investigate the function of Akr1c18 in wound healing, we first focused on the SCAD assay. Expansion of the fascial region can be observed in SCADs transduced with AAV6-Akr1c18-T2A-GFP (Fig 4.5A). Masson's Trichrome staining showed a slightly thicker fascial layer in Akr1c18 overexpressing SCAD (Fig 4.5B). However, there was no obvious difference in ECM composition between GFP and Akr1c18 overexpressing SCAD (Fig 5B). The expression of $\alpha$-SMA-expressing in Akr1c18 over-expressing SCADs was similar in control SCADs, as demonstrated by immunofluorescence staining(Fig 4.5C). To examine the effect of Akr1c18 on cell migration, we performed time-lapse 3D imaging using multiphoton microscope. We first noticed morphological differences in Akr1c18-transfected fibroblasts, which showed an elongated shape (Fig 4.5E,G). Furthermore, the Akr1c18-transduced fibroblasts moved at a relatively low rate compared with the control GFP group. It is known that resting or quiescent fibroblasts are inert and are recognized as spindle-shaped single cells (Kalluri, 2016). Akr1c18-transfected fibroblasts have a extreme spindle shape, implying Akr1c18 overexpression might influence the state of fibroblast. The swollen fascia in Akr1c18 SCAD may be due to the reductase activity of this gene (Ishida, Hirabayashi, Suzuki, Yamanouchi, & Nishihara, 2003).

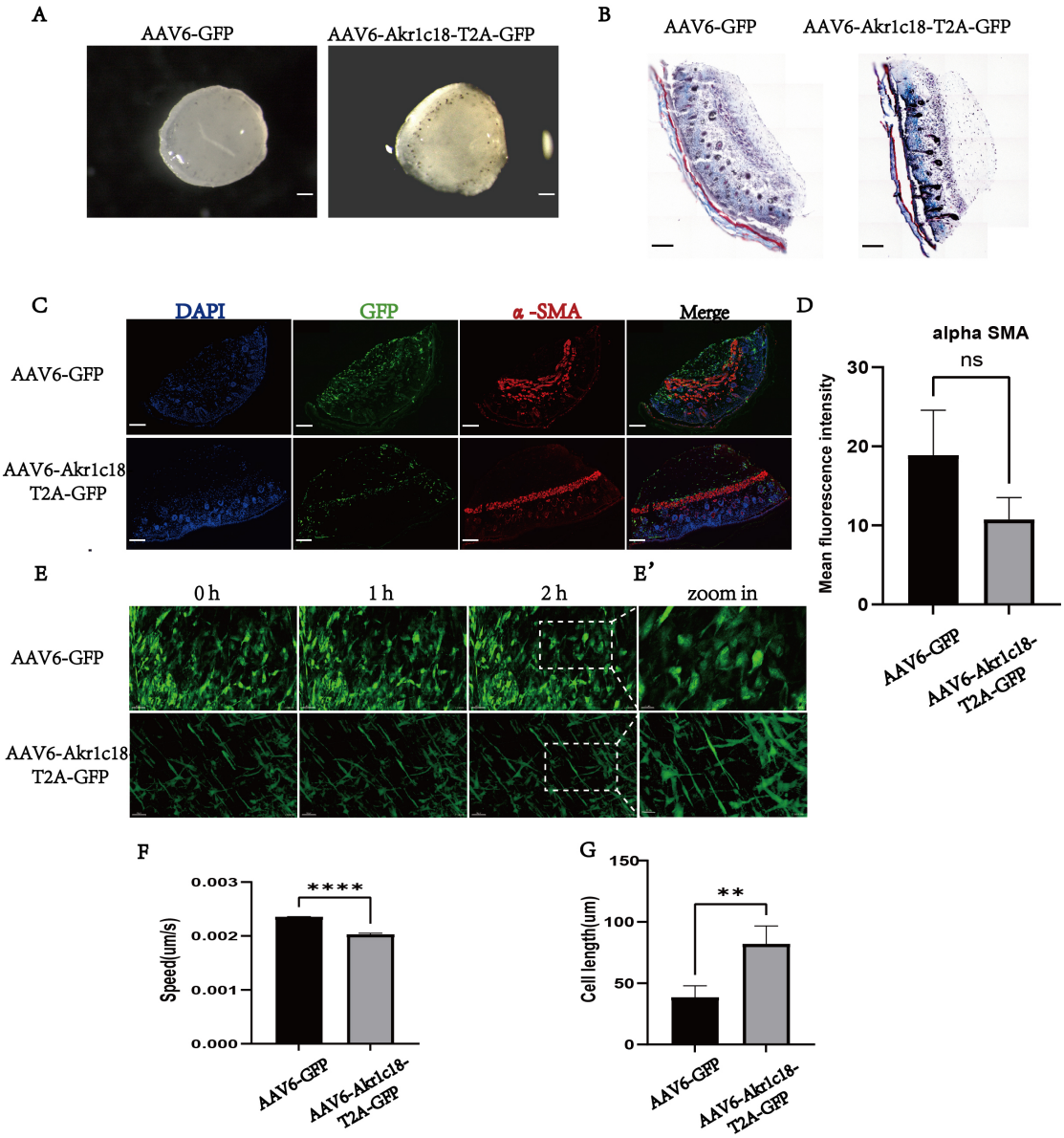


**Figure 4.5 the overexpression of Akr1c18 in wound healing in the SCAD model.**

(A) The bright-field image of SCAD transfected with AAV coding GFP and Akr1c 18 respectively. (B) Trichrome staining of SCAD transfected with AAV coding GFP or Akr1c18. (C) Histology analysis of GFP and alpha SMA in the AAV transfected SCAD. (D) quantification of the a-SMA expression in SCAD. (E) Time snapshot of transfected SCAD at different time points.(E') the zoom in image of transfected fibroblast.(F) Velocity analysis of fibroblast in the AAV transfected SCAD. (G) quantification of the cell length of fibroblast in SCAD. Scar Bar A, B, C, = 150 um, E = 40 um, E' = 20um.

## 4.6 Investigate the role of Akr1c18 in wound healing in the excisional wound model

To further investigate the function of Akr1c18 in wound healing, we performed excisional wounds on newborn mice. Akr1c18 overexpression did not show a significant influence on the wound closure (Fig 4.6 A, B). Further histology showed no significant difference in ECM composition (Fig 4.6 C). The staining of ki67 in both groups was much limited to the only hair follicle region, rather than the wound area (Fig 4.6 D). The overexpression of Akr1c18 does not affect cell proliferation.

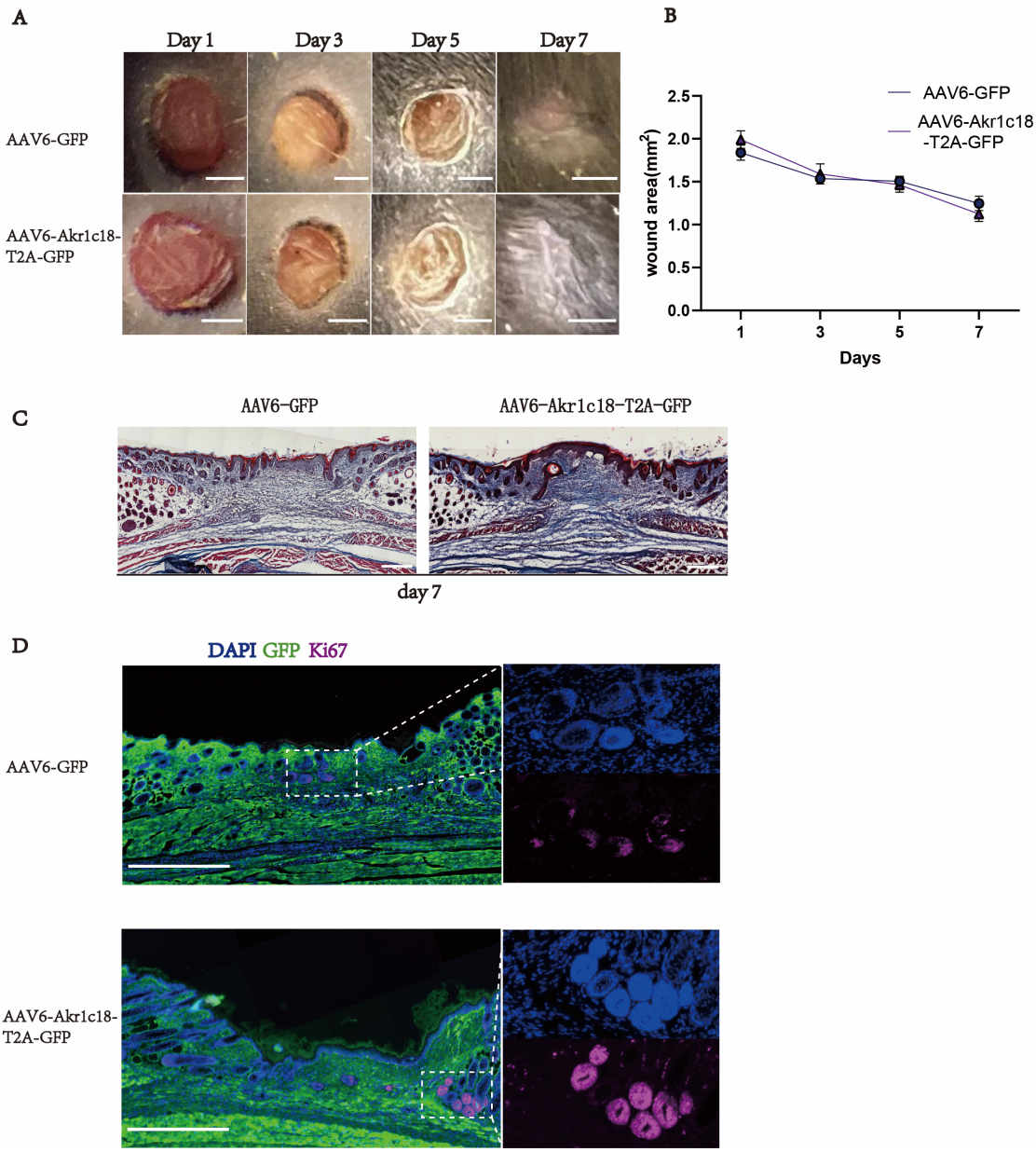


**Figure 4.6 Investigate the role of Akr1c18 in wound healing using an excisional wound model**

(A) Wound area at different timepoint during wound healing. (B) Quantity analysis of the wound at different timepoint during wound healing. (C) Trichrome staining of samples from the AAV injected newborn pups at day 7 past wound. (D) Histology analysis of Ki 67 of samples from the AAV injected newborn pups. Scar bar A = 1000 um, C = 250 um, D = 500 um.

## 4.7 Bioinformatic analysis Akr1c18 expression pattern during the wound healing

To investigate the function of Akr1c18 at single-cell resolution, we analyzed the single-cell

RNA sequencing data during skin wound repair. To remove the interference of the other cell lineages, we isolated the wound fibroblasts at different time-points after wounding using negative depletion strategy (Walmsley et al., 2016). Based on the single-cell RNA sequence data, seven transcriptionally distinct clusters were revealed (Figure 4.7 A). Akr1c18 is mainly expressed in the fascia fibroblast and pro-myofibroblast (Figure 4.7 B). Overlaying time course information on the tSNE plot revealed that AKr1c 18 expression went down gradually during the wound repair process (Figure 4.7 C).

Akr1c18 is mainly expressed in fascia fibroblast and pro-myofibroblast, in which collagen expression is very low (Figure 4.7 F). Akr1c18 functions as a progesterone inactivator, almost undetectable in the late-stage wound myofibroblast group (Figure 4.7C). We found that several progesterone metabolism and secretion relevant genes, including Runx1, Inaba, and scp2 highly expressed in the myofibroblast (Figure 4.7 D). In addition, we also found that progesterone response genes including Tgfb2, Abhd2, Ubeca, Cav1, and Rnf4 are expressed at relatively high level in myofibroblast and Pro-Myofibroblast (Figure 4.7 E). One possible explanation is that low Akr1c 18 expression in mature wound fibroblasts causes elevated progesterone level in the skin and elevated progesterone-response gene expression in wound fibroblasts. All of these suggested that progesterone pathways might also be involved in the wound healing process.

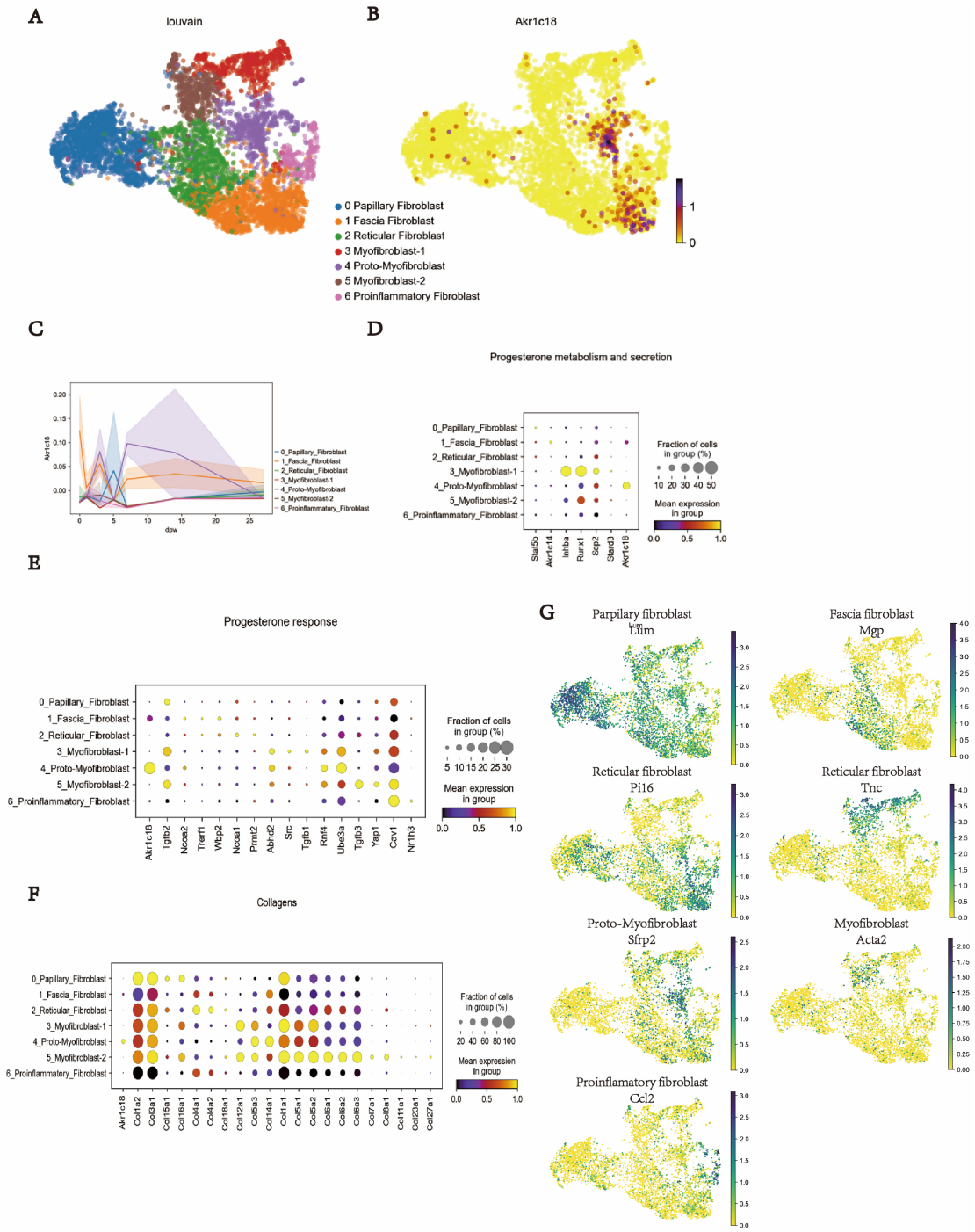


**Figure 4.7 The single-cell sequencing analysis of the wound fibroblast during wound healing**

(A) Annotated cell-identity clusters found by Louvain clustering visualized for the fascia and wound fibroblast. (B) The expression of Akr1c18 in the annotated cell-identity clusters. (C) The expression of akr1c18 in the seven annotated wound fibroblast clusters along pseudo-time trajectories. (D) Bubble plot comparing expression of progesterone metabolism and secretion across the seven annotated fibroblast clusters. The comparison of progesterone response (E) and collagen (F) across the seven annotated wound fibroblast clusters.(G) Feature plots of expression distribution for selected cluster-specific genes.

# 5. Discussions

## 5.1 Transduction optimization of AAV vectors for in vitro application

AAV is rarely used for in vitro genetic manipulation. In our project, we do a series of optimizing to increase the transfection efficiency. We first identified AAV6 serotype capable of the SCAD transfection. At first, we tested the AAV-DJ serotype, which has outstanding transfection in a series of in vitro cell line.  To our surprise, AAV-DJ is unable to transfect the SCAD tissue. The 3D transfection in tissue is usually more difficult than the traditional 2D transfection. And SCAD tissue can also not be seen as a mixture of several in vitro cell types.

Although AAV6 can transfected SCAD samples in vitro, the real efficiency is very low. Given that other viral vectors like lentiviruses and retroviruses, require the addition of the cationic polymer-Polybreme to facilitate in vitro transfection, we set out to seek the chemical compounds which have a similar function. We found sodium butyrate was found to greatly boost transfection efficiency (Fig 4.3B, C). Sodium butyrate is a histone deacetylase inhibitor. The concentration used in our experiments was 20 mM, which could lead to potential side effects and affect the experiments. However, in our experiments, we did not find any obvious change in SHG and collagen caused by the addition of sodium butyrate (Fig 4.3E). However, it is still necessary to check the effect of sodium butyrate on some other factors related to scar formation, such as cell migration and proliferation, etc. Sodium butyrate enhanced AAV transfection greatly in vitro, so perhaps a similar effect could be

seen in vivo. However, the addition of Sodium butyrate is unnecessary. Using the appropriate AAV serotype, transfection efficiency is also very effective for animal experiments.

Capsid engineering seems to be the most reliable method to enhance the transduction of AAV However, designing, screen and identifying the novel AAV serotype is usually quite time consuming and labor-intensive. AAV transduction in vitro could be enhanced by physical methods such as magnetic transfection and centrifugal transfection. These methods enhance transfection by physically enhancing the interaction of AAV particles with infected cells, and thus reduce the viral titer used. This approach can be combined with the addition of sodium butyrate, which may reduce the dosage of sodium butyrate to prevent the potential undesired side effects.

## 5. 2 The importance of the proper design of AAV transgenic plasmids, which is often overlooked.

Typically, when using AAV for gene transfer, viral titration is a very important factor. The dose of AAV administered to animals is carefully calculated. The most common way to improve the transfection efficiency of AAV in animal experiments is to increase the amount of virus used. However, this was not always true. A high virus dose is detrimental to experimental animals as it can cause a strong immune response, which will interfere with interpretation of the experimental results. In the murine excisional wound model, excessive virus titers are injurious to the mice and are likely to result in scarring outcomes. Optimize

the overexpression cassette is simple solution, which is relatively easy but is often ignored.

To investigate the effect of target genes on fibroblast migration in the SCAD model, we first used a design in which the target gene and GFP form a fusion protein via a linker (Figure 4.4.1 A). The advantage of this approach is that the subcellular localization of the target gene can be observed. In contrast to the control vectors only express GFP, the vectors expressing Akr1c18-GFP fusion protein had very low GFP expression (Figure 4.4.1 B, C). Based on this, I decided to change the design of the transgenic plasmid. I set out to use either a 2a self-cleaving peptide or an IRES to achieve co-expression of GFP and the target gene

The 2a strategy also has its limitations. Mechanistically, the 2a peptide is a linker that can cause an interruption in the translation process, i.e. ribosomal skipping, resulting in the C-terminus of the target gene containing several amino acid residues of the 2a linker, which may inhibit the function of the target gene. The prerequisite of the 2A strategy is that the important functional domains or conserved regions of the target gene are not located at its C-terminus. We examined the structure of Akr1c18 and found it is suitable for the 2A strategy. However, we cannot exclude the possibility that the amino acid residues of the 2a linker may affect the function of Akr1c18. To avoid this problem, the IRES linker can be used to achieve co-expression of the target gene and GFP. However, the GFP expression using IRES is much lower than that of 2A (Figure 4.4.2 B) and the size of the IRES is much larger than 2a, which limits the capacity of the AAV vector. The most ideal strategy is very

likely to be viral vectors based on the bidirectional mammalian promoters, which can express reporter GFP and target gene at the two opposite directions independently. Bidirectional promoter can avoid the drawbacks of 2A or IRES based strategy very well.

## 5.3 The role of Akr1c18 and progesterone in wound healing.

Recent studies in our laboratory have revealed that in wound healing, the superficial fascia fibroblasts migrate upward and differentiate into myofibroblasts, repairing the wound. To explore this mechanism, we performed single-cell RNA sequencing of wound fibroblasts along the wound repair process. We found that the expression of the gene Akr1c18 was very high in fascial fibroblasts and pro-myofibroblasts, but decreased dramatically at the late wound stage (Figure 8 A, B). Akr1c18 overexpression is very likely have a negative effect on wound healing.

In the SCAD model, overexpression of Akr1c18 has been shown to have a negative effect on fibroblast migration. However, Akr1c18 overexpression has a very limited effect on myofibroblast differentiation and scar formation, and wound closure. The only thing can be confirmed is that the function of Akr1c18 in wound healing is closely linked to the progesterone pathway. The single-cell sequencing showed that some genes related to progesterone response, such as cav1, were highly expressed in wound fibroblast, which also show very low level of Akr1c18 expression (Figure 8E). Considering that the main function of Akr1c18 is the progesterone inactivator, low Akr1c18 expression in mature wound fibroblast might cause elevated progesterone level in the skin and further elevated

progesterone-response gene expression in wound fibroblasts.

It is proven that progesterone can inhibit inflammatory innate immune responses and progesterone receptor is present in many immune cells. At normal state, the reduced expression of Akr1c18 in wound fibroblasts is very likely to aimed to enhance the anti-inflammatory effects of progesterone on immune cells, thus facilitating the transition from the inflammatory to the proliferative phase in wound repair. Conversely, overexpression of Akr1c18 is likely to reduce the effect of progesterone and let the wound repair trapped in the stage of inflammatory stage. However, we did not see this effect.

One possible reason is that we are conducting experiment on new born pups, rather than the adult mice. First of all, the scRNA analysis is based on samples from the adult mice, rather than the pups. The wound repair mechanism might be different between adult mice and newborn pups. Furthermore, progesterone in the skin is most likely derived from cholesterol in dermal white adipose tissue (DWAT). DWAT is abundant in adult mice, but almost absent in the skin of newborn pups. The overexpression of Akr1c18 has no downstream target, thus having limited effect in wound repair.

# Reference


ADAMS, R. L. C., & BIRD, R. J. (2009). Review article: Coagulation cascade and therapeutics update: Relevance to nephrology. Part 1: Overview of coagulation, thrombophilias and history of anticoagulants. *Nephrology, 14*(5), 462-470. doi:https://doi.org/10.1111/j.1440-1797.2009.01128.x

Atchison, R. W., Casto, B. C., & Hammon, W. M. (1965). ADENOVIRUS-ASSOCIATED DEFECTIVE VIRUS PARTICLES. *Science, 149*(3685), 754-756. doi:10.1126/science.149.3685.754

Baldo, A., van den Akker, E., E Bergmans, H., Lim, F., & Pauwels, K. (2013). General considerations on the biosafety of virus-derived vectors used in gene therapy and vaccination. *Current gene therapy, 13*(6), 385-394.

Bartlett, J. S., Wilcher, R., & Samulski, R. J. (2000). Infectious entry pathway of adeno-associated virus and adeno-associated virus vectors. *Journal of virology, 74*(6), 2777-2785. doi:10.1128/jvi.74.6.2777-2785.2000

Chung, D. C., Fogelgren, B., Park, K. M., Heidenberg, J., Zuo, X., Huang, L., . . . Lipschutz, J. H. (2011). Adeno-Associated Virus-Mediated Gene Transfer to Renal Tubule Cells via a Retrograde Ureteral Approach. *Nephron extra, 1*(1), 217-223. doi:10.1159/000333071

Colella, P., Ronzitti, G., & Mingozzi, F. (2018). Emerging issues in AAV-mediated in vivo gene therapy. *Molecular Therapy-Methods & Clinical Development, 8*, 87-104.

Collaco, R. F., Cao, X., & Trempe, J. P. (1999). A helper virus-free packaging system for recombinant adeno-associated virus vectors. *Gene, 238*(2), 397-405. doi:10.1016/s0378-1119(99)00347-9

Correa-Gallegos, D., Jiang, D., Christ, S., Ramesh, P., Ye, H., Wannemacher, J., . . . Rinkevich, Y. (2019). Patch repair of deep wounds by mobilized fascia. *Nature, 576*(7786), 287-292. doi:10.1038/s41586-019-1794-y

Ding, W., Zhang, L., Yan, Z., & Engelhardt, J. F. (2005). Intracellular trafficking of adeno-associated viral vectors. *Gene Therapy, 12*(11), 873-880. doi:10.1038/sj.gt.3302527

Driskell, R. R., Lichtenberger, B. M., Hoste, E., Kretzschmar, K., Simons, B. D., Charalambous, M., . . . Watt, F. M. (2013). Distinct fibroblast lineages determine dermal architecture in skin development and repair. *Nature, 504*(7479), 277-281. doi:10.1038/nature12783

Drouin, L. M., & Agbandje-McKenna, M. (2013). Adeno-associated virus structural biology as a tool in vector development. *Future virology, 8*(12), 1183-1199. doi:10.2217/fvl.13.112

Ellis, S., Lin, E. J., & Tartar, D. (2018). Immunology of Wound Healing. *Current Dermatology Reports, 7*(4), 350-358. doi:10.1007/s13671-018-0234-9

Fang, C.-C., Wu, C.-F., Liao, Y.-J., Huang, S.-F., Chen, M., & Chen, Y.-M. A. (2018). AAV serotype 8-mediated liver specific GNMT expression delays progression of hepatocellular carcinoma and prevents carbon tetrachloride-induced liver damage. *Scientific Reports, 8*(1), 13802. doi:10.1038/s41598-018-30800-3

Ferrari, F. K., Samulski, T., Shenk, T., & Samulski, R. J. (1996). Second-strand synthesis is a rate-limiting step for efficient transduction by recombinant adeno-associated virus vectors. *Journal of virology, 70*(5), 3227-3234. doi:10.1128/jvi.70.5.3227-3234.1996

Fore, J. (2006). A review of skin and the effects of aging on skin structure and function. *Ostomy Wound Manage, 52*(9), 24-35; quiz 36-27.

George Broughton, I., Janis, J. E., & Attinger, C. E. (2006). Wound healing: an overview. *Plastic and reconstructive surgery, 117*(7S), 1e-S-32e-S.

Ghosh, A., Yue, Y., Lai, Y., & Duan, D. (2008). A Hybrid Vector System Expands Adeno-associated Viral Vector Packaging Capacity in a Transgene-independent Manner. *Molecular Therapy, 16*(1), 124-130. doi:https://doi.org/10.1038/sj.mt.6300322

Gonzalez, A. C. d. O., Costa, T. F., Andrade, Z. d. A., & Medrado, A. R. A. P. (2016). Wound healing - A literature review. *Anais brasileiros de dermatologia, 91*(5), 614-620. doi:10.1590/abd1806-4841.20164741

Grieger, J. C., & Samulski, R. J. (2005). Adeno-associated virus as a gene therapy vector: vector development, production and clinical applications. *Adv Biochem Eng Biotechnol, 99*, 119-145.

Grimm, D., Lee, J. S., Wang, L., Desai, T., Akache, B., Storm, T. A., & Kay, M. A. (2008). In vitro and in vivo gene therapy vector evolution via multispecies interbreeding and retargeting of adeno-associated viruses. *Journal of virology, 82*(12), 5887-5911. doi:10.1128/jvi.00254-08

Gurtner, G. C., Werner, S., Barrandon, Y., & Longaker, M. T. (2008). Wound repair and regeneration. *Nature, 453*(7193), 314-321. doi:10.1038/nature07039

Hall, O. J., & Klein, S. L. (2017). Progesterone-based compounds affect immune responses and susceptibility to infections at diverse mucosal sites. *Mucosal Immunology, 10*(5), 1097-1107. doi:10.1038/mi.2017.35

Hart, J. (2002). Inflammation. 1: Its role in the healing of acute wounds. *J Wound Care, 11*(6), 205-209. doi:10.12968/jowc.2002.11.6.26411

Hoggan, M. D., Blacklow, N. R., & Rowe, W. P. (1966). Studies of small DNA viruses found in various adenovirus preparations: physical, biological, and immunological characteristics. *Proc Natl Acad Sci U S A, 55*(6), 1467-1474. doi:10.1073/pnas.55.6.1467

Im, S., Lee, E. S., Kim, W., Song, J., Kim, J., Lee, M., & Kang, W. H. (2000). Expression of progesterone receptor in human keratinocytes. *J Korean Med Sci, 15*(6), 647-654. doi:10.3346/jkms.2000.15.6.647

Ishida, M., Hirabayashi, K., Suzuki, M., Yamanouchi, K., & Nishihara, M. (2003). Cloning and chromosomal localization of mouse 20α-hydroxysteroid dehydrogenase gene. *Journal of Reproduction and Development, 49*(1), 79-85.

Jiang, D., Christ, S., Correa-Gallegos, D., Ramesh, P., Kalgudde Gopal, S., Wannemacher, J., . . . Rinkevich, Y. (2020). Injury triggers fascia fibroblast collective cell migration to drive scar formation through N-cadherin. *Nature Communications, 11*(1), 5653. doi:10.1038/s41467-020-19425-1

Jiang, D., Correa-Gallegos, D., Christ, S., Stefanska, A., Liu, J., Ramesh, P., . . . Rinkevich, Y. (2018). Two succeeding fibroblastic lineages drive dermal development and the transition from regeneration to scarring. *Nature Cell Biology, 20*(4), 422-431. doi:10.1038/s41556-018-0073-8

Lee, G. K., Maheshri, N., Kaspar, B., & Schaffer, D. V. (2005). PEG conjugation moderately protects adeno-associated viral vectors against antibody neutralization. *Biotechnol Bioeng, 92*(1), 24-34. doi:10.1002/bit.20562

Liu, Z., Chen, O., Wall, J. B. J., Zheng, M., Zhou, Y., Wang, L., . . . Liu, J. (2017). Systematic comparison of 2A peptides for cloning multi-genes in a polycistronic vector. *Scientific Reports, 7*(1),

2193. doi:10.1038/s41598-017-02460-2

Lundstrom, K. (2004). Gene therapy applications of viral vectors. *Technol Cancer Res Treat, 3*(5), 467-477. doi:10.1177/153303460400300508

McCarty, D. M., Monahan, P. E., & Samulski, R. J. (2001). Self-complementary recombinant adeno-associated virus (scAAV) vectors promote efficient transduction independently of DNA synthesis. *Gene Therapy, 8*(16), 1248-1254. doi:10.1038/sj.gt.3301514

Mingozzi, F., & High, K. A. (2013). Immune responses to AAV vectors: overcoming barriers to successful gene therapy. *Blood, 122*(1), 23-36. doi:10.1182/blood-2013-01-306647

Müller, O. J., Kaul, F., Weitzman, M. D., Pasqualini, R., Arap, W., Kleinschmidt, J. A., & Trepel, M. (2003). Random peptide libraries displayed on adeno-associated virus to select for targeted gene therapy vectors. *Nature Biotechnology, 21*(9), 1040-1046. doi:10.1038/nbt856

Nance, M. E., & Duan, D. (2015). Perspective on Adeno-Associated Virus Capsid Modification for Duchenne Muscular Dystrophy Gene Therapy. *Human gene therapy, 26*(12), 786-800. doi:10.1089/hum.2015.107

Naso, M. F., Tomkowicz, B., Perry, W. L., 3rd, & Strohl, W. R. (2017). Adeno-Associated Virus (AAV) as a Vector for Gene Therapy. *BioDrugs, 31*(4), 317-334. doi:10.1007/s40259-017-0234-5

Nonnenmacher, M., & Weber, T. (2012). Intracellular transport of recombinant adeno-associated virus vectors. *Gene Therapy, 19*(6), 649-658. doi:10.1038/gt.2012.6

Nour, S., Baheiraei, N., Imani, R., Khodaei, M., Alizadeh, A., Rabiee, N., & Moazzeni, S. M. (2019). A review of accelerated wound healing approaches: biomaterial- assisted tissue remodeling. *Journal of Materials Science: Materials in Medicine, 30*(10), 120. doi:10.1007/s10856-019-6319-6

Pelletier, G., & Ren, L. (2004). Localization of sex steroid receptors in human skin. *Histol Histopathol, 19*(2), 629-636. doi:10.14670/hh-19.629

Piekorz, R. P., Gingras, S., Hoffmeyer, A., Ihle, J. N., & Weinstein, Y. (2005). Regulation of progesterone levels during pregnancy and parturition by signal transducer and activator of transcription 5 and 20alpha-hydroxysteroid dehydrogenase. *Mol Endocrinol, 19*(2), 431-440. doi:10.1210/me.2004-0302

Plikus, M. V., Guerrero-Juarez, C. F., Ito, M., Li, Y. R., Dedhia, P. H., Zheng, Y., . . . Cotsarelis, G. (2017). Regeneration of fat cells from myofibroblasts during wound healing. *Science, 355*(6326), 748-752. doi:10.1126/science.aai8792

Pryadkina, M., Lostal, W., Bourg, N., Charton, K., Roudaut, C., Hirsch, M. L., & Richard, I. (2015). A comparison of AAV strategies distinguishes overlapping vectors for efficient systemic delivery of the 6.2 kb Dysferlin coding sequence. *Molecular therapy. Methods & clinical development, 2*, 15009-15009. doi:10.1038/mtm.2015.9

Rinkevich, Y., Walmsley, G. G., Hu, M. S., Maan, Z. N., Newman, A. M., Drukker, M., . . . Longaker, M. T. (2015). Skin fibrosis. Identification and isolation of a dermal lineage with intrinsic fibrogenic potential. *Science (New York, N.Y.), 348*(6232), aaa2151-aaa2151. doi:10.1126/science.aaa2151

Roberto, A. J. (2016). Pharmacology for Women' s Health. *The Yale Journal of Biology and Medicine, 89*(2), 269-270. Retrieved from https://www.ncbi.nlm.nih.gov/pmc/articles/PMC4918866/

Rodrigues, M., Kosaric, N., Bonham, C. A., & Gurtner, G. C. (2019). Wound Healing: A Cellular Perspective. *Physiological reviews, 99*(1), 665-706. doi:10.1152/physrev.00067.2017

Sami, D., Heiba, H., & Abdellatif, A. (2018). Wound Healing Models; A Systematic Review of Animal and Non-Animal Models. *Wound Medicine, 24*, 8-17. doi:10.1016/j.wndm.2018.12.001

Samulski, R. J., Zhu, X., Xiao, X., Brook, J. D., Housman, D. E., Epstein, N., & Hunter, L. A. (1991). Targeted integration of adeno-associated virus (AAV) into human chromosome 19. *Embo j, 10*(12), 3941-3950.

Shirley, J. L., de Jong, Y. P., Terhorst, C., & Herzog, R. W. (2020). Immune Responses to Viral Gene Therapy Vectors. *Molecular Therapy, 28*, 709 - 722.

Shook, B. A., Wasko, R. R., Mano, O., Rutenberg-Schoenberg, M., Rudolph, M. C., Zirak, B., . . . Horsley, V. (2020). Dermal Adipocyte Lipolysis and Myofibroblast Conversion Are Required for Efficient Skin Repair. *Cell Stem Cell, 26*(6), 880-895.e886. doi:https://doi.org/10.1016/j.stem.2020.03.013

Singer, A. J., & Clark, R. A. F. (1999). Cutaneous Wound Healing. *New England Journal of Medicine, 341*(10), 738-746. doi:10.1056/nejm199909023411006

Sinha, M., Sen, C. K., Singh, K., Das, A., Ghatak, S., Rhea, B., . . . Roy, S. (2018). Direct conversion of injury-site myeloid cells to fibroblast-like cells of granulation tissue. *Nature Communications, 9*(1), 936. doi:10.1038/s41467-018-03208-w

Stecco, C., Macchi, V., Porzionato, A., Duparc, F., & De Caro, R. (2011). The fascia: the forgotten structure. *Ital J Anat Embryol, 116*(3), 127-138.

van Lieshout, L. P., Domm, J. M., Rindler, T. N., Frost, K. L., Sorensen, D. L., Medina, S. J., . . . Wootton, S. K. (2018). A Novel Triple-Mutant AAV6 Capsid Induces Rapid and Potent Transgene Expression in the Muscle and Respiratory Tract of Mice. *Molecular therapy. Methods & clinical development, 9*, 323-329. doi:10.1016/j.omtm.2018.04.005

Vergnes, L., Phan, J., Stolz, A., & Reue, K. (2003). A cluster of eight hydroxysteroid dehydrogenase genes belonging to the aldo-keto reductase supergene family on mouse chromosome 13. *Journal of Lipid Research, 44*(3), 503-511. doi:https://doi.org/10.1194/jlr.M200399-JLR200

Walmsley, G. G., Maan, Z. N., Hu, M. S., Atashroo, D. A., Whittam, A. J., Duscher, D., . . . Longaker, M. T. (2016). Murine Dermal Fibroblast Isolation by FACS. *J Vis Exp*(107). doi:10.3791/53430

Wang, D., Tai, P. W. L., & Gao, G. (2019). Adeno-associated virus vector as a platform for gene therapy delivery. *Nature Reviews Drug Discovery, 18*(5), 358-378. doi:10.1038/s41573-019-0012-9

Weinmann, J., & Grimm, D. (2017). Next-generation AAV vectors for clinical use: an ever-accelerating race. *Virus Genes, 53*(5), 707-713. doi:10.1007/s11262-017-1502-7

Weinmann, J., Weis, S., Sippel, J., Tulalamba, W., Remes, A., El Andari, J., . . . Grimm, D. (2020). Identification of a myotropic AAV by massively parallel in vivo evaluation of barcoded capsid variants. *Nature Communications, 11*(1), 5432. doi:10.1038/s41467-020-19230-w

Westhaus, A., Cabanes-Creus, M., Rybicki, A., Baltazar, G., Navarro, R. G., Zhu, E., . . . Lisowski, L. (2020). High-Throughput In Vitro, Ex Vivo, and In Vivo Screen of Adeno-Associated Virus Vectors Based on Physical and Functional Transduction. *Human gene therapy, 31*(9-10), 575-589. doi:10.1089/hum.2019.264

Wetendorf, M., & DeMayo, F. J. (2014). Progesterone receptor signaling in the initiation of

pregnancy and preservation of a healthy uterus. *The International journal of developmental biology, 58*(2-4), 95-106. doi:10.1387/ijdb.140069mw

Wu, J., Zhao, W., Zhong, L., Han, Z., Li, B., Ma, W., . . . Srivastava, A. (2007). Self-complementary recombinant adeno-associated viral vectors: packaging capacity and the role of rep proteins in vector purity. *Human gene therapy, 18*(2), 171-182. doi:10.1089/hum.2006.088

Wu, Z., Yang, H., & Colosi, P. (2010). Effect of genome size on AAV vector packaging. *Molecular therapy : the journal of the American Society of Gene Therapy, 18*(1), 80-86. doi:10.1038/mt.2009.255

Wu, Z., Yang, H., & Colosi, P. (2010). Effect of genome size on AAV vector packaging. *Mol Ther, 18*(1), 80-86. doi:10.1038/mt.2009.255

Xu, Z., Yue, Y., Lai, Y., Ye, C., Qiu, J., Pintel, D. J., & Duan, D. (2004). Trans-splicing adeno-associated viral vector-mediated gene therapy is limited by the accumulation of spliced mRNA but not by dual vector coinfection efficiency. *Human gene therapy, 15*(9), 896-905. doi:10.1089/hum.2004.15.896

Xue, M., & Jackson, C. J. (2015). Extracellular Matrix Reorganization During Wound Healing and Its Impact on Abnormal Scarring. *Advances in wound care, 4*(3), 119-136. doi:10.1089/wound.2013.0485

Yousef, H., Alhajj, M., & Sharma, S. (2022). Anatomy, Skin (Integument), Epidermis. In *StatPearls*. Treasure Island (FL): StatPearls Publishing



Zhang, Y., Li, H., Min, Y. L., Sanchez-Ortiz, E., Huang, J., Mireault, A. A., . . . Olson, E. N. (2020). Enhanced CRISPR-Cas9 correction of Duchenne muscular dystrophy in mice by a self-complementary AAV delivery system. *Sci Adv, 6*(8), eaay6812. doi:10.1126/sciadv.aay6812

# Acknowledgment

My doctoral study in Germany was a very important experience in my life. The first person I would like to sincerely thank is Dr. Christina. Without her help, I would not have had the opportunity to study in Germany. She is very dedicated to her students. The short time I spent in her lab was the most enjoyable part of my doctoral period.

I sincerely thank Dr. Yuval Rinkevich for accepting me into his lab to conduct cutting-edge scientific research. I had the opportunity to learn a lot, which exceeded my expectations. I sincerely thank him for providing very good experimental conditions for my project. I would like to thank my TAC members: Prof. Behr and Dr. Anne. They provided me with excellent guidance for my project and enabled me to complete my Ph.D.

I thank all colleagues in our lab, especially Ms. Sandra Schiener. She is always willing to help when I am in trouble, which is already beyond her duty. I would like to thank Donovan, Jiakuan, who helped me to solve the technical problems in my project, and Pushkar and Haifeng for their essential support in my experiments.  I am grateful to all my colleagues who work at our Lung Institute and are always willing to help if they can. I would like to thank the colleagues at the animal facility, who take care of the experimental animals. I would also like to thank the animals who died in my experiments and contributed data to my thesis.

The person I would most like to thank is my girlfriend, who cook great dishes for me and arrange many extraordinary trips. Thanks for her joining me. We have many happy times.

I would like to thank my parents and our country. Our country has provided me with an opportunity to study abroad. I also look forward to returning from my studies to build my country. I would like to thank my parents for their silent dedication. I would like to express my heartfelt thanks to all those who helped me during my studies in Germany.

# Affidavit

zhu, shaohua

Surname, first name

Address

I hereby declare, that the submitted thesis entitled

is my own work. I have only used the sources indicated and have not made unauthorised use of services of a third party. Where the work of others has been quoted or reproduced, the source is always given.

I further declare that the dissertation presented here has not been submitted in the same or similar form to any other institution for the purpose of obtaining an academic degree.

| Munich,12-10-2022 | Shaohua Zhu |
| --- | --- |
| Place, Date | Signature doctoral candidate |

# Confimation of congruency between printed and electronic version of the doctoral thesis

Doctoral Candidate: shaohua zhu

Address:

I hereby declare that the electronic version of the submitted thesis, entitled

is congruent with the printed version both in content and format.

| munich, 12-10-2022 | Shaohua Zhu |
|---|---|
| Place, Date | Signature doctoral candidate |

# List of Publication

Connexin43 gap junction drives fascia mobilization and repair of deep skin wounds.

Wan L, Jiang D., Correa-Gallegos D., Ramesh P., Zhao J., Ye H, et al.

Matrix Biol. 2021;97:58-71.